quence of a dye artifact, double or triple immunolabelling was performed sequentially. After washing three times in PBS with 0.1% Triton X-100, the slices were mounted with Permafluor (Immunotech, France). Each specimen was analysed three-dimensionally with a z-axis interval of 0.87–0.88 μm under a conventional confocal laser microscope (LSM510META, Zeiss, Thornwood, NY, USA) equipped with 40 × objectives unless otherwise noted. The images were corrected for brightness and contrast using conventional software (LSM Image Browser version 3.2, Zeiss and Photoshop version 6.0, Adobe Systems Inc, San Jose, CA, USA).

Results

Cellular architecture of granule cell layer

Hippocampal slices prepared from postnatal rats were cultured for several weeks. The gross appearances of slices between 2 and 6 weeks of plating (Fig. 1, A2 and A3) were similar to those from the living intact animal (Fig. 1, A1) as noted in the previous studies (Stoppini *et al.*, 1991; Okada *et al.*, 1995). To further investigate the cellular architecture of the slice culture, neurons were identified by the expression of neuronal nuclei antigen (NeuN), which is expressed specifically in the nucleus of mature neuron with unknown functions (Mullen *et al.*, 1992). Similar to the living animal (Fig. 1, B1), GCL cells and pyramidal cell layer (PCL) cells of the CA1–4 region were preserved for as long as 6 WIV (Fig. 1, B2 and B3). The GCL was usually compact and clearly discriminated from the surrounding tissues in the suprapyramidal region whereas neurons formed a loose cluster and occasionally migrated out from the slices in the infrapyramidal region (e.g. Fig. 1, B2). To identify the GCL, all the following experiments were limited to the suprapyramidal region.

Next, we investigated whether the laminar arrangement of the slice culture assures optimal hippocampal networks. In the hippocampus *in vivo* the MF gives rise to fine collaterals with numerous small boutons in the hilus and traverses the apical dendritic shafts of CA3 pyramidal cells in a narrow band called the stratum lucidum (Henze *et al.*, 2000). Presynaptic boutons of the MF contain an exceptionally high concentration of zinc in the synaptic vesicles (Frederickson *et al.*, 2000). To identify the MF projection we applied a zinc sensitive fluorescent indicator, TSQ, which brightly

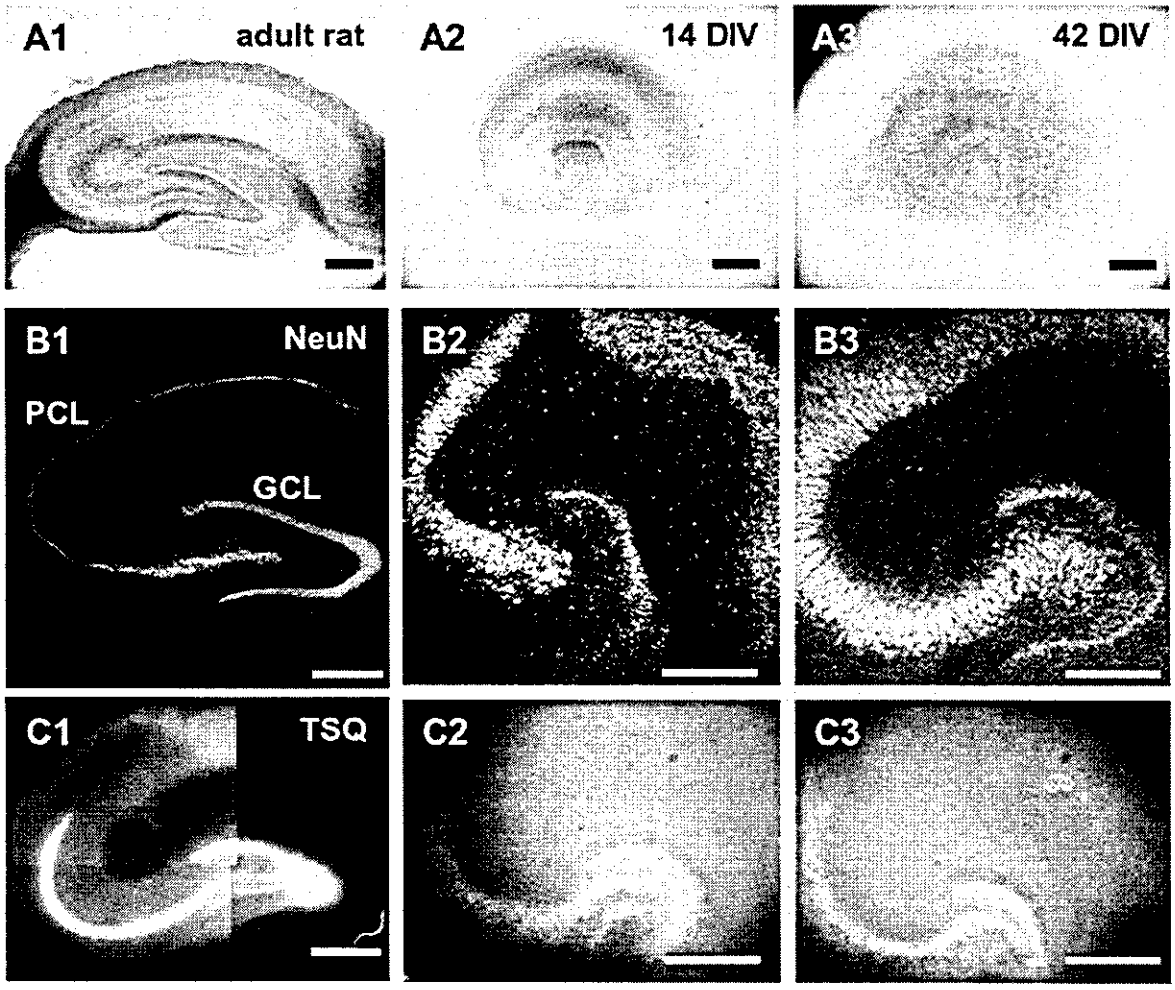

FIG. 1. The cellular architecture of rat hippocampal slice cultures. (A1–3) Plain views of hippocampal slice and its culture: the acute slice from an adult rat (A1), 14 DIV slice culture (A2) and 42 DIV slice culture (A3). (B1–3) The organizations of neuronal layers: the acute slice from adult rat (B1), 14 DIV slice culture (B2) and 42 DIV slice culture (B3). Neurons were immunolabelled with anti-NeuN, a neuron-specific marker. Note the presence of both the dentate granule cell layers (GCLs) and the CA1–4 pyramidal cell layers (PCLs). (C1–3) The laminar arrangements of mossy fibre (MF) projections: the acute slice from adult rat (C1), 14 DIV slice culture (C2) and 42 DIV slice culture (C3). The MFs and their terminals were visualized with a zinc-sensitive fluorescent indicator, *N*-(6-methoxy-8-quinolyl)-*p*-toluenesulphonamide (TSQ). The pattern of MF projections in the slice cultures is similar to that *in vivo*. Scale bars, 0.5 mm.

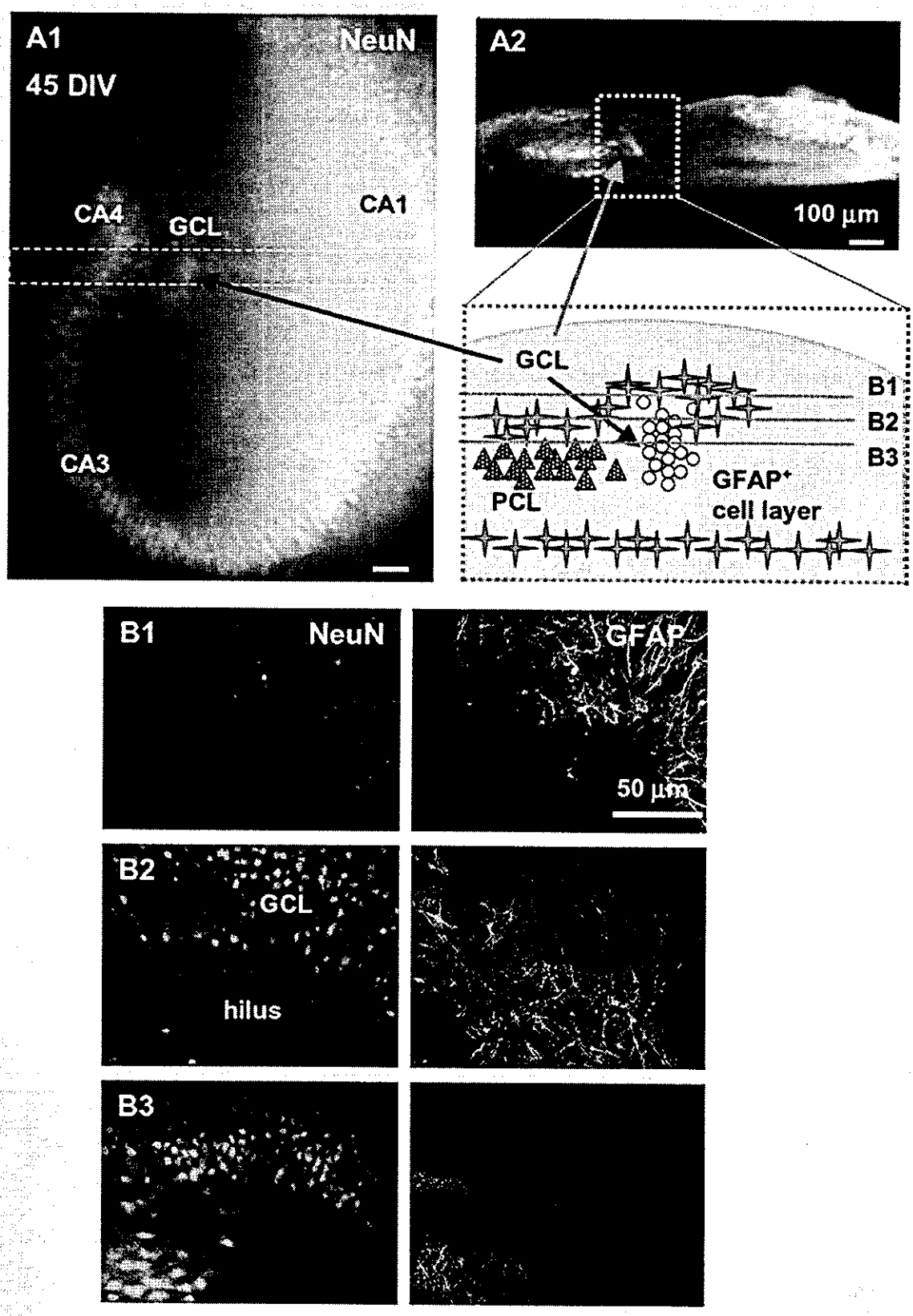

FIG. 2. Three-dimensional architecture of the dentate gyrus. (A1 and 2) The distribution of neurons in a 45 DIV slice culture: the horizontal (A1) and vertical (A2) appearances. Neurons were immunolabelled with anti-NeuN. The region between broken lines in A1 is viewed from the side in A2. The cartoon of cytoarchitecture corresponds to the square region in A2. The dotted lines, B1–3 correspond to the following panels B1–3, respectively. Neurons in the GCL and PCL are indicated by circles and triangles, respectively, and astrocytes by stars. The unidentified structure of slice culture is coloured in grey. (B1–3) The three-dimensional distribution of neurons and astrocytes in the dentate gyrus of a slice culture 6 μm above the layer of GCL (B1), the layer where GCL first appears (B2) and 6 μm below B2 (B3). The double immunofluorescent images of anti-NeuN (left), anti-GFAP (right) were obtained by using confocal microcopy.

labels the following regions (Fig. 1, C1): hilus of dentate gyrus; CA3 suprapyramidal and infrapyramidal layer. These brightly fluorescent regions were almost identical to those obtained with other metal-histochemical methods like Timm staining method (Frederickson *et al.*, 1987; Vogt *et al.*, 2000). Throughout the cultivation period TSQ brightly labelled these regions in some slices: 40.0% ($n = 25$) at 14 DIV (Fig. 1, C2); and 31.5% ($n = 108$) at 42 DIV (Fig. 1, C3). However, MF projections were obscure in others, probably through the massive reorganization of axonal trajectories or the ectopic projections in slice cultures (Robain *et al.*, 1994; Gutierrez & Heinemann, 1999). As the presence of robust MF projections is an indication of the preservation of efficient hippocampal architecture, all the following experiments were carried out after TSQ identification of MF projections.

Three-dimensional architecture of the dentate gyrus

Even when hippocampal slice cultures had preserved laminar structures for several weeks, the slices were flattened within the first week and maintained their thickness for subsequent weeks, as reported previously (Buchs *et al.*, 1993). To determine the position and thickness of the GCL in the slice culture, slices at 45 DIV were cut in a perpendicular plane to the Millicell-CM membrane along the CA1–4 axis, which had been previously fixed and immunolabelled for anti-NeuN (Fig. 2, A1). Slices had thinned to 179 ± 12 μm ($n = 11$; Fig. 2, A2) from the previous thickness of 350 μm. The PCL was stretched horizontally at CA1, as reported previously (Buchs *et al.*, 1993), whereas the GCL (thickness of tens of micrometres) was buried in the middle of the slice and was densely packed with neurons with small-sized nuclei.

To resolve the three-dimensional cytoarchitecture of the dentate gyrus, the culture slices at 45 DIV were immunolabelled with anti-NeuN and anti-glial fibrillary acidic protein (GFAP), specific antibodies to one of intermediate filament proteins and one of selective markers of astrocytes and radial glia (Ludwin *et al.*, 1976; Seri *et al.*, 2001), and inspected by using confocal laser scanning microscopy from the surface to the bottom (see Fig. 2 cartoon). There was a layer of GFAP-positive cells just above the GCL (Fig. 2, B1). In the layer containing the GCL, there was a dense cluster of NeuN-positive small nuclei, surrounded by GFAP-positive cells (Fig. 2, B2). In the deeper layer, NeuN-positive cells were found in the GCL as well as the PCL at CA4 (Fig. 2, B3). Although we did not determine the type of cells located under the neuronal somatic area, GFAP-positive processes sometimes tightly formed a thin layer in a vicinity of the Millicell-CM membrane.

Differentiation of endogenous progenitors in slice cultures

To investigate whether endogenous progenitors exist intrinsically and actually differentiate into neurons in the slice culture, we added BrdU, a thymidine analogue, to the culture medium. As BrdU is incorporated into nuclei during the S-phase, it should label the newly generated cells in slice cultures. The phenotype of BrdU-labelled cells was identified immunohistochemically using antibodies to neuronal or glial markers, under higher magnification. Usually, the suprapyramidal region of the GCL was set in the centre of the optical field, and the optical planes above and in the GCL were examined. In the case of slices at 45 DIV, triple immunofluorescent labelling (anti-BrdU, anti-NeuN and anti-GFAP) was carried out to identify the specific phenotypes of BrdU-labelled cells.

One week after BrdU treatment, many BrdU-labelled cells were found in and around the GCL, and occasionally appeared as pairs being opposed each other (Fig. 3, B1 and B3, arrowheads), but were coexpressed with neither NeuN (Fig. 3, A1–3) nor microtubule-associated protein 2 (MAP2; Fig. 3, B1–3), one of the cytoskeletal proteins expressed specifically in neuronal cell bodies and dendrites (Bernhardt & Matus, 1984). Many of these BrdU-labelled nuclei did not associate with GFAP-positive structures overlaying the GCL (Fig. 3, C1-3). However, under close inspection of three-dimensional structures, a few BrdU-labelled nuclei were encapsulated by the GFAP-positive fibres (asterisk). Some BrdU- and GFAP-positive cells had characteristic short processes (Fig. 3C, insets). These BrdU-labelled cells might also include non-neuronal and non-glial cells as microglia and fibroblasts although both cells are supposed to be few in the region around the GCL (Raineteau *et al.*, 2004).

Four weeks after treatment, confocal images revealed that some of the BrdU-labelled nuclei were coexpressed with NeuN in the GCL (Fig. 4, A1–3, arrowheads). These cells were not immunoreactive with anti-GFAP (Fig. 4, A4). The coexpression of BrdU and NeuN was examined three-dimensionally under higher magnification (Fig. 4B). In the layer overlaying the GCL, there were some BrdU-labelled nuclei surrounded by GFAP-positive processes (Fig. 4, C1–3, arrows). These cells were not immunolabelled by anti-NeuN (Fig. 4, C4).

Visualization of endogenous neurogenesis in living slices

The BrdU-labelling method has several disadvantages for the study of neurogenesis. Neurogenesis is only retrospectively identified in fixed tissues. Labelling with BrdU is not sufficient to prove that a given cell has divided because BrdU is a marker of DNA synthesis rather than of cell division (Rakic, 2002). BrdU-labelling alone does not reveal morphological characteristics of the newly generated cells as BrdU is incorporated into only their nuclei. Finally, the cellular and physiological features of living cells are difficult to investigate. To overcome these disadvantages, we marked endogenous progenitors in living slice cultures with EGFPs using retrovirus vectors, which were injected locally into the suprapyramidal region of the GCL. As the retroviruses infect only dividing cells and their genes are incorporated into the host's genomic DNA, newly divided cells and their descendants would specifically express EGFP.

From daily observations of the injected sites under fluorescent microscopy, the EGFP-expressing cells showed a tendency to increase in number between 1- and 2-weeks post-inoculation (Fig. 5, A1 and A2). The number of EGFP-expressing cells was followed up in six slices in which more than four EGFP-expressing cells were identified in the DGL 1 week after retrovirus vector inoculation and was even increased in the next 1–3 weeks (Fig. 5B). The relative number increased to 253 ± 58% (mean ± SEM; $n = 5$) in 1 week and to 296 ± 104% ($n = 4$) in 2 weeks. As our retrovirus vector is replication-incompetent, the EGFP-expressing cells proliferated as a result of mitosis. In the first 1–2-weeks post-inoculation, the typical EGFP-expressing cells were small with short processes (Fig. 5A), being reminiscent of the undifferentiated cells that had recently appeared. Indeed, three-dimensional analysis of confocal images revealed that 36 ± 4% (mean ± SEM; four slices, sum of double positive cells/total EGFP-expressing cells = 45/128) of these cells expressed nestin, one of intermediate filaments expressed specifically in neuroblasts and myoblasts (Lendahl *et al.*, 1990) and a putative neural precursor markers (see also Fig. S1 in Supplementary material). By contrast, the EGFP-expressing cells have neither neuronal appearances nor detectable NeuN immunoreactivities in these early

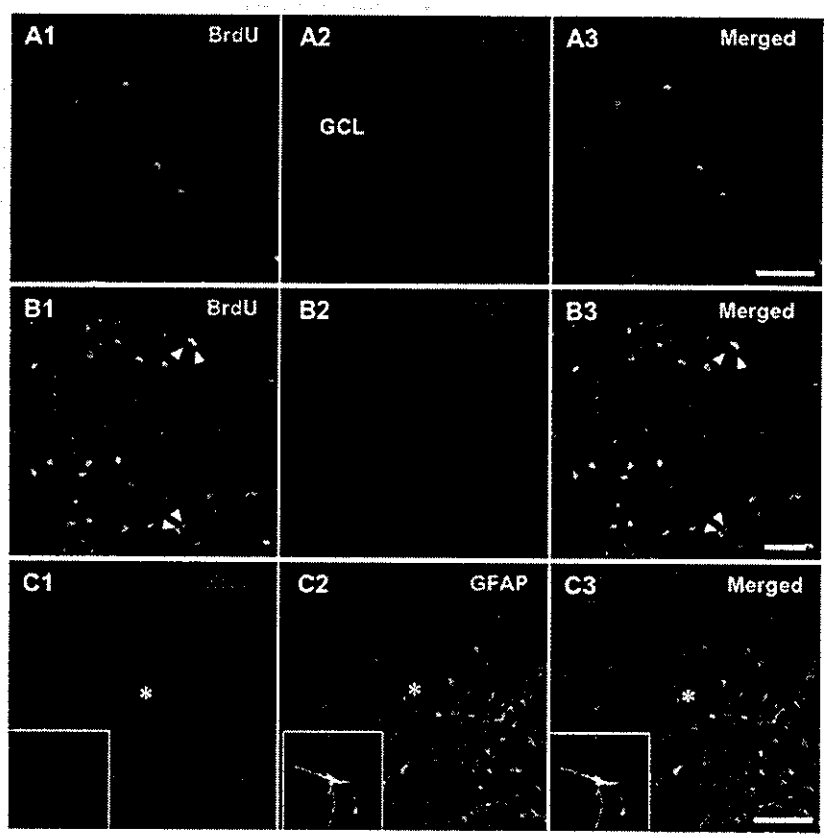
A1
BrdU
A2
GCL
A3
Merged
B1
BrdU
B2
B3
Merged
C1
C2
GFAP
C3
Merged

FIG. 3.

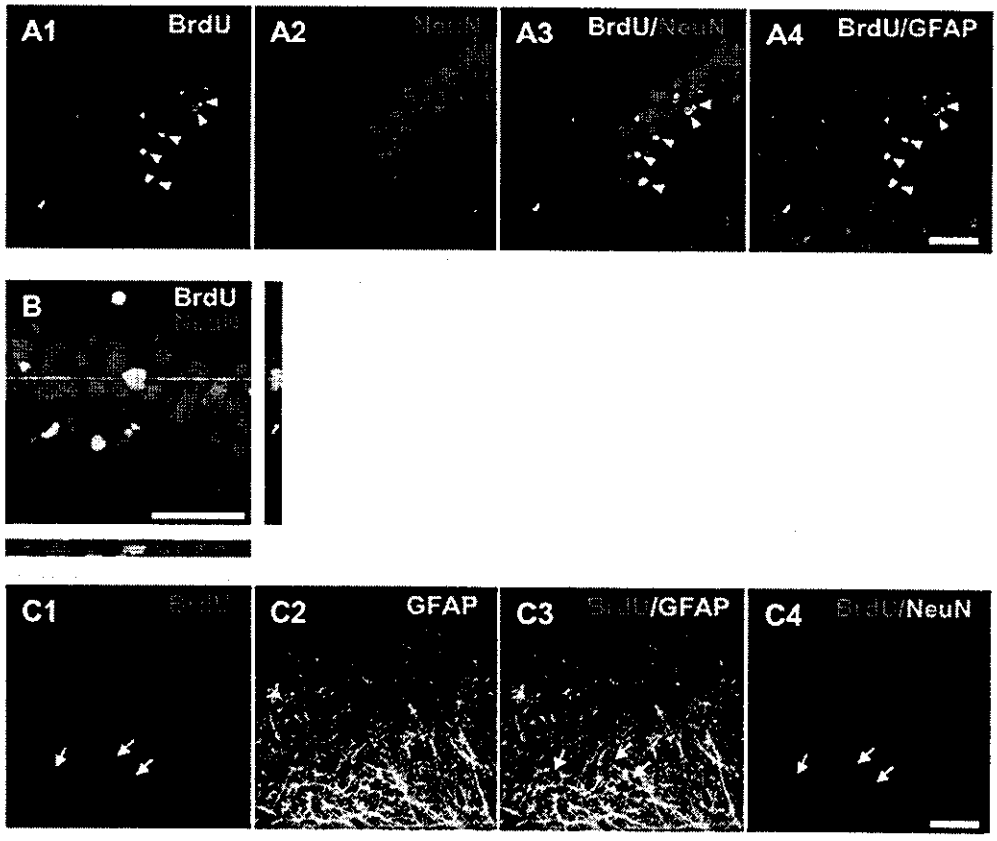
A1
BrdU
A2
A3
BrdU/NeuN
A4
BrdU/GFAP
B
BrdU
C1
C2
GFAP
C3
C4
BrdU/NeuN

FIG. 4.

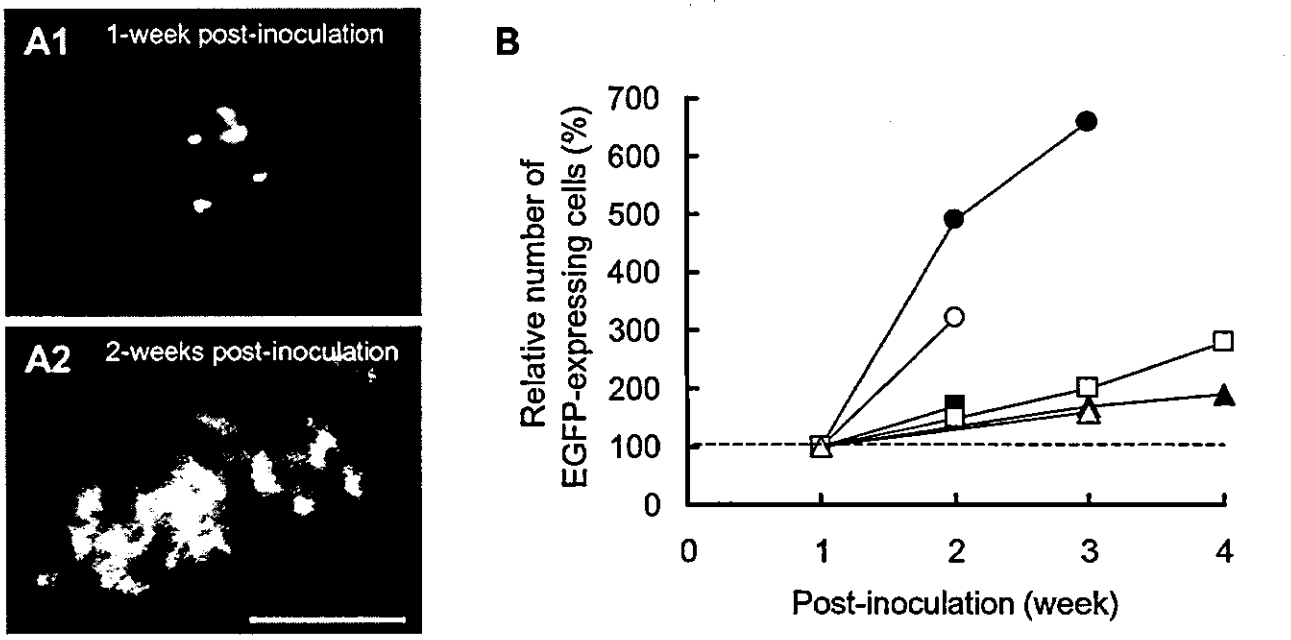

FIG. 5. Proliferation of enhanced green fluorescent protein (EGFP)-expressing cells after retrovirus vector inoculation. (A) The EGFP-expressing cells in the dentate gyrus at 1- (A1) and 2-weeks (A2) post-inoculation in the same place. Scale bar, 50 μm. (B) The number of EGFP-labelled cells in the dentate gyrus was counted, normalized to that seen at 1-week postinoculation and plotted against time. Each symbol represents an identical slice culture ($n = 6$).

postinoculation periods, indicating that our retrovirus vectors would not transfect mature neurons.

Some of the EGFP-expressing cells extended processes in the late WIV

Three-dimensional analysis of confocal images were investigated for phenotypes of EGFP-expressing cells 4 weeks after inoculation. Typical EGFP-expressing cells were seen in the GCL with several dendrite-like processes (Fig. 6A) and one elongated axon-like process (Fig. 6A, arrowheads) bearing putative synaptic boutons (Fig. 6A, arrow). The coexpression of EGFP and NeuN (Fig. 6B) was examined three-dimensionally under higher magnification (Fig. 6C). Some of these cells were immunoreactive to anti-NeuN and were incorporated in the normal architecture of GCL (Fig. 6A and B). Some EGFP-expressing cells represented early phenotypes of differentiation into neurons in the GCL with short processes and immunolabelled with antibodies to Tuj1 (Fig. 6D), one of the cytoskeletal proteins expressed specifically in immature neurons (Lee *et al.*, 1990). The detailed morphology of neuron-like EGFP-expressing cells also varied, as shown in Fig. 6A and B. Some dendrite-like processes extended to z-axis directions whereas others were horizontal. Some axon-like processes extended in the direction of CA3 pyramidal cells whereas in others it was the opposite. We tracked these axons for a considerable length but were unable to find the final destinations. To test if these EGFP-expressing cells have phenotypes of GCL neurons, the coexpression of EGFP and calbindin D28K, one of calcium binding proteins expressed specifically in some types of neurons including DGL cells (Baimbridge & Miller, 1982; Bousez-Dumesnil *et al.*, 1989) was examined three-dimensionally under a higher magnification (Fig. 6E). Indeed, there were the neuron-like EGFP-expressing cells immunoreactive to calbindin D28K in the DGL. These results are consistent with the notion that the slice cultures intrinsically retain a neurogenic potential qualitatively similar to the hippocampus in the living animal.

To investigate the occurrence of neuronal differentiation, retrovirus vectors were injected on the same day in the same place of the suprapyramidal region of the DGL of 14 DIV slice cultures derived from 10 littermates of either gender and prepared on the same day. Four weeks after inoculation, 14 slice cultures were selected for analysis of phenotypes because they had numbers (> 10) of EGFP-expressing cells. The immunoreactivity to anti-NeuN was investigated

FIG. 3. Phenotypes of newly generated cells in the dentate gyrus one week after incorporation of 5-bromodeoxyuridine (BrdU). (A1–3) The double immunofluorescent confocal images of GCL: anti-BrdU (A1, green), anti-NeuN (A2, red) and the merge (A3). (B1–3) The double immunofluorescent confocal images of GCL: anti-BrdU (B1, green), anti-MAP2 (B2, red) and the merge of both (B3). The double arrowheads indicate mitotic figures. (C1–3) The double immunofluorescent confocal images of the dentate gyrus: anti-BrdU (C1, red), anti-GFAP (C2, green) and the merge (C3). The asterisk indicates the BrdU-labelled GFAP-positive cell. Inset shows another BrdU-labelled GFAP-positive cell with processes clearly visible. Scale bars, 50 μm.

FIG. 4. Phenotypes of newly generated cells in the dentate gyrus four weeks after incorporation of BrdU. (A1–4) The triple immunofluorescent confocal images of GCL: anti-BrdU (A1, green), anti-NeuN (A2, red), the merge of both (A3) and the merge of anti-BrdU and anti-GFAP (blue) images (A4). The arrowheads indicate the newly generated neurons which are both BrdU-labelled and NeuN-positive. (B) Three-dimensional confocal micrograph showing a typical BrdU/NeuN-immunoreactive cell. The x–z and y–z images were accompanied. Note that BrdU distributes in the nucleus of the NeuN-positive cell in the DGL. (C1–4) Triple immunofluorescent confocal images of the layer overlaying GCL: anti-BrdU (C1, red), anti-GFAP (C2, green), the merge (C3) and the merge of anti-BrdU and anti-NeuN (blue) images (C4). The arrows indicate the BrdU-labelled GFAP-positive cell. Scale bars, 50 μm.

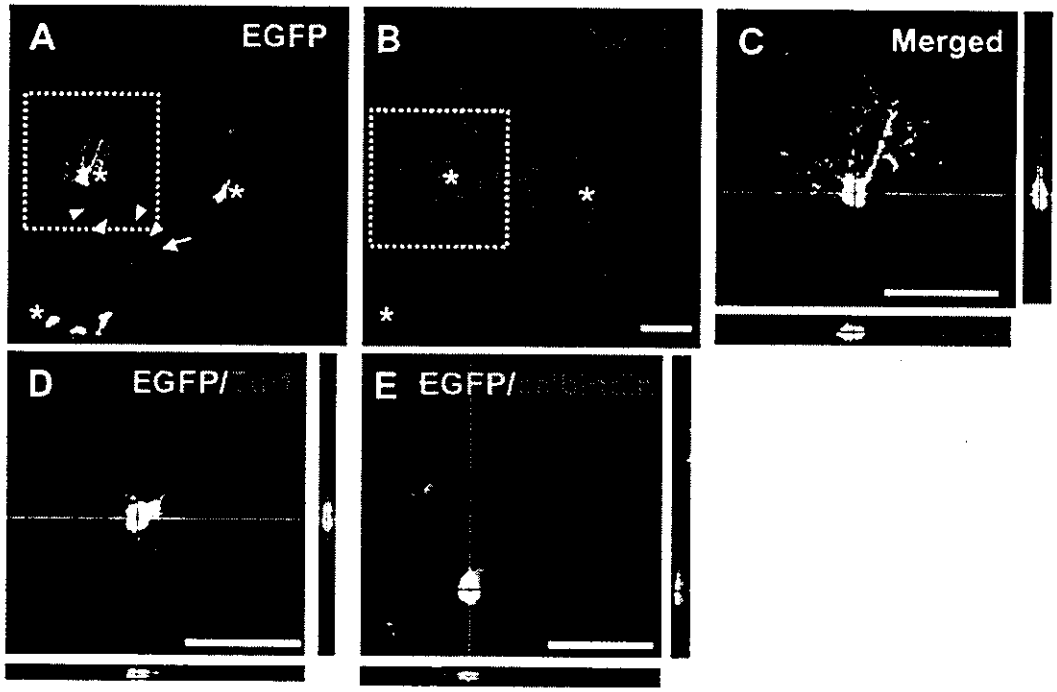

FIG. 6. Emergence of neuronal phenotypes in EGFP-expressing cells four weeks after retrovirus vector inoculation. (A and B) The double immunofluorescent confocal images of GCL: anti-EGFP (A, green), anti-NeuN (B, red). Typical EGFP-expressing NeuN-positive cells bear dendrite-like processes and an axon-like process (arrowheads) with a terminal bouton-like structure (arrow). EGFP-expressing cells that are immunoreactive with anti-NeuN are indicated by asterisks. (C) Three-dimensional analysis of a NeuN-positive EGFP-expressing cell. A rectangular region in A and B were merged and enlarged with x–z and y–z images. (D) Three-dimensional analysis of a double immunofluorescent confocal image of GCL: anti-EGFP (green) and anti-Tuj1 (red). The x–z and y–z images were accompanied. (E) Three-dimensional analysis of a double immunofluorescent confocal image of GCL: anti-EGFP (green); anti-calbindin D28K (red). The x–z and y–z images were accompanied. Scale bars, 50 μm.

in four slices. The NeuN-positive cells were found in the range of 10–40% of the EGFP-expressing cells. In total 23 of 91 EGFP-expressing cells were NeuN-positive (25%). The Tuj1-positive cells were in the range of 10–40% of the EGFP-expressing cells (four slices) and 23 of 94 EGFP-expressing cells in total (24%). Therefore, some but not all newly divided cells express neuronal phenotypes (see Fig. S1 in Supplementary material). In fact, in this series of experiments, the GFAP-positive cells were in the range of 10–40% of the EGFP-expressing cells (three slices) and 33 of 103 EGFP-expressing cells in total (32%). The nestin-positive cells were in the range of 10–40% of the EGFP-expressing cells (four slices) and 36 of 133 EGFP-expressing cells in total (27%).

Discussion

We made several observations reinforcing the previous study that postnatal hippocampal slice cultures preserve endogenous neuronal progenitor cells in the dentate gyrus, in which new neurons are spontaneously generated (Raineteau *et al.*, 2004). With BrdU used to label dividing cells, we found that some BrdU-labelled cells acquire phenotypes of mature neurons in the following four weeks. Using retrovirus vectors, we found that in 4 weeks some EGFP-expressing cells also acquire phenotypes of mature neurons extending dendrites and axon-like processes.

Differences between labelling methods

One of our new findings is that EGFP-expressing cells proliferated in the explanted hippocampus during the cultivation period between 1- and 4-week postinoculation (Fig. 5). This is in contrast to the observation that the number of BrdU-labelled cells has a tendency to decrease in days after early proliferation (Hayes & Nowakowski, 2002). Since BrdU is incorporated into DNA during mitosis, its density diminishes during the following cell divisions (Dayer *et al.*, 2003). Therefore, the descendents of highly proliferative cells would become negligible regarding BrdU immunoreactivity. Alternatively, the undifferentiated cells might be selected for survival before differentiation with massive cell death (Gould *et al.*, 1999a). Either way, it is generally accepted that BrdU preferentially labels the immediately post-mitotic cells during the period of drug exposure. By contrast, the retrovirus vector transduction reveals a different population of cells, the newly divided ones and their descendents.

Neurogensis in the slice culture system

In this study some BrdU-labelled cells in the GCL were also positive for NeuN, a marker of mature neurons (Fig. 4A and B). These observations are consistent with reports of *in vivo* preparations (Kuhn *et al.*, 1996; Eriksson *et al.*, 1998; Kornack & Rakic, 1999) and slice culture systems (Raineteau *et al.*, 2004), and imply that intrinsic neural progenitors are present in the hippocampal slice culture of 2 WIV and that some of their descendents differentiate into GCL neurons.

Four weeks after retrovirus vector inoculation, about one-quarter of EGFP-expressing cells were immunoreactive with anti-NeuN and about one-quarter with anti-Tuj1, a marker of immature neurons. These numbers compare with those in *in vivo* experiments: 2–25% for anti-NeuN and 15–30% for anti-Tuj1, although these values do depend on the

behavioural conditions of the mice (van Praag *et al.*, 2002). The EGFP-expressing NeuN-positive cells were found primarily in the GCL of the slice culture (Fig. 6A and B). Similarly, most of the BrdU-labelled NeuN-positive cells were found in the GCL, being consistent with the previous study (Raineteau *et al.*, 2004). Therefore, the newly generated neurons are distributed similarly to that reported in postnatal mammals *in vivo* (Kuhn *et al.*, 1996; Eriksson *et al.*, 1998; Kornack & Rakic, 1999). We also found that some EGFP-expressing cells were immunoreactive to calbindin D28K, a marker of GCL neurons (Fig. 6E), being consistent with the *in vivo* studies (Kuhn *et al.*, 1996).

In the adult rodent brain, neurogenic stem cells are present in the subgranular zone of the hippocampus and the newly generated neurons preferentially distribute close to the subgranular zone in the GCL *in vivo* (Cameron *et al.*, 1993; Alvarez-Buylla & Lim, 2004) and in the thin slice culture using the roller-tube methods (Raineteau *et al.*, 2004). However, in our rather thick slice culture system using the interface methods (Stoppini *et al.*, 1991) we found no particular patterns in the appearance of BrdU-labelled/EGFP-expressing NeuN-positive cells in the GCL. Therefore, the three-dimensional structure of the neurogenic niche appears to be somewhat reorganized in our slice culture system.

Undifferentiated cells

One week after mitosis the large number of BrdU-labelled cells appeared to be undifferentiated because they were coexpressing with neither neuronal markers such as NeuN and MAP2 nor astrocyte markers such as GFAP (Fig. 3). Four weeks after retrovirus vector inoculation the EGFP-expressing cells consisted of various phenotypes: NeuN-positive (Fig. 6C); Tuj1-positive (Fig. 6D); GFAP-positive; and nestin-positive (see Supplementary material). Immediately after mitosis the descendants express nestin, an intermediate filament protein found in neuroepithelial stem cells, but usually lose it within a week during maturation (Palmer *et al.*, 2000). Therefore, those nestin-postive EGFP-expressing cells may have a history of recent mitosis. Although we did not investigate phenotypes of nestin-negative EGFP-expressing cells, neuronal and glial progenitors, microglia, endothelial cells and fibroblasts would be included (Raineteau *et al.*, 2004).

Neurons have been shown to express Tuj1 early in differentiation (Lee *et al.*, 1990; Menezes & Luskin, 1994) whereas they express NeuN after maturation (Mullen *et al.*, 1992). Some of our EGFP-expressing neurons showed phenotypes of either early or late stages of differentiation. It is, therefore, possible that there are lineages of self-renewing neural precursor cells that are neurogenic (Palmer *et al.*, 1997) as a consequence of asymmetric cell division (Alvarez-Buylla *et al.*, 2001; Fishell & Kriegstein, 2003). Alternatively, neurons might remain undifferentiated for weeks, and become mature by triggering signals, e.g. synaptic contacts. It is also possible that some of newly generated cells undergo apotosis before maturation (Gould & Gross, 2002) although the EGFP-expressing cells have a tendency to increase in number as a whole as late as 4 weeks after transduction (Fig. 5). Careful follow up of a single pair of EGFP-expressing cells in the slice culture system would shed light on this problem.

Gliogenesis in the slice culture system

Some BrdU-labelled cells expressed GFAP, a molecular marker of astrocytes (Fig. 4C) and about one-third of the EGFP-expressing cells were also positive for GFAP 4 weeks after retrovirus vector inoculation (see Supplementary material). These observations are consistent with previous *in vivo* experiments that cells positive for both BrdU and GFAP are present in the dentate hilus–subgranular zone in the hippocampus (Kempermann *et al.*, 1997). However, the GFAP-positive cells encompass a diverse group of cells (Seri *et al.*, 2001) including terminally differentiated astrocytes (Goldman, 2003) and radial glial cells, which have neurogenic potential (Seri *et al.*, 2001). It has been also suggested that neural precursor cells generally have a history of expressing GFAP at least once (Seri *et al.*, 2001; Kronenberg *et al.*, 2003). Experiments using other molecular markers are necessary to further classify these GFAP-positive cells.

There remains another issue as to whether the GFAP-positive cells and the NeuN-positive cells derived from the same progenitor. This could be tested in our slice culture system by following up a single pair of EGFP-expressing cells using retrovirus vector transduction.

Concluding remarks

Two independent studies, ours and that of Raineteau *et al.* (2004) would make it unequivocal that endogenous neural progenitor cells are indeed present in the slice culture system and spontaneously generating new neurons postnatally. Using the retrovirus vector transduction method in combination, the slice culture system would enable follow up of the newly divided cells for a long period.

Supplementary material

The following supplementary material may be found on: http://www.blackwellpublishing.com/products/journals/suppmat/EJN/EJN3721/EJN3721sm.htm

Fig. S1. Emergence of non-neuronal phenotypes in EGFP-expressing cells in the dentate gyrus around the suprapyramidal region of the GCL after retrovirus vector inoculation.

Acknowledgements

We are grateful to H. Minami for technical assistance R. Araki and K. Miyazaki for helpful comments and to M. Ohara (Fukuoka) for language assistance.

Abbreviations

BrdU, 5-bromodeoxyuridine; DIV, days *in vitro*; EGFP, enhanced green fluorescent protein; GFAP, glial fibrillary acidic protein; GCL, granule cell layer; MAP2, microtubule-associated protein 2; MF, mossy fibre; NeuN, neuronal nuclei antigen; PCL, pyramidal cell layer; TSQ, *N*-(6-methoxy-8-quinolyl)-*p*-toluenesulphonamide; Tuj1, neuron-specific β-III tubulin; WIV, weeks *in vitro*.

References

Altman, J. & Das, G.D. (1965) Autoradiographic and histological evidence of postnatal hippocampal neurogenesis in rats. *J. Comp. Neurol.*, **124**, 319–336.

Alvarez-Buylla, A., Garcia-Verdugo, J.M. & Tramontin, A.D. (2001) A unified hypothesis on the lineage of neural stem cells. *Nat. Rev. Neurosci.*, **2**, 287–293.

Alvarez-Buylla, A. & Lim, D.A. (2004) For the long run: maintaining germinal niches in the adult brain. *Neuron*, **41**, 683–686.

An, D.S., Koyanagi, Y., Zhao, J.-Q., Akkina, R., Bristol, G., Yamamoto, N., Zack, J.A. & Chen, I.S.Y. (1997) High-efficiency transduction of human lymphoid progenitor cells and expression in differentiated T cells. *J. Virol.*, **71**, 1397–1404.

An, D.S., Morizono, K., Li, Q.X., Mao, S.H., Lu, S. & Chen, I.S. (1999) An inducible human immunodeficiency virus type 1 (HIV-1) vector which effectively suppresses HIV-1 replication. *J. Virol.*, **73**, 7671–7677.

Baimbridge, K.G. & Miller, J.J. (1982) Immunohistochemical localization of calcium-binding protein in the cerebellum, hippocampal formation and olfactory bulb of the rat. *Brain Res.*, **245**, 223–229.

Benninger, F., Beck, H., Wernig, M., Tucker, K.L., Brustle, O. & Scheffler, B. (2003) Functional integration of embryonic stem cell-derived neurons in hippocampal slice cultures. *J. Neurosci.*, **23**, 7075–7083.

Bernhardt, R. & Matus, A. (1984) Light and electron microscopic studies of the distribution of microtubule-associated protein 2 in rat brain: a difference between dendritic and axonal cytoskeletons. *J. Comp. Neurol.*, **226**, 203–221.

Bousez-Dumesnil, N., Thomasset, M. & Ben-Ari, Y. (1989) Calbindin-D28K in hippocampal organotypic cultures. *Brain Res.*, **486**, 165–169.

Buchs, P.-A., Stoppini, L. & Muller, D. (1993) Structural modification associated with synaptic development in area CA1 of rat hippocampal organotypic cultures. *Dev. Brain Res.*, **71**, 81–91.

Cameron, H.A., Woolley, C.S., McEwen, B.S. & Gould, E. (1993) Differentiation of newly born neurons and glia in the dentate gyrus of the adult rat. *Neuroscience*, **56**, 337–344.

Dailey, M.E., Buchanan, J., Bergles, D.E. & Smith, S.J. (1994) Mossy fiber growth and synaptogenesis in rat hippocampal slices in vitro. *J. Neurosci.*, **14**, 1060–1078.

Dayer, A.G., Ford, A.A., Cleaver, K.M., Yassaee, M. & Cameron, H.A. (2003) Short-term and long-term survival of new neurons in the rat dentate gyrus. *J. Comp. Neurol.*, **460**, 563–572.

Eriksson, P.S., Perfilieva, E., Bjork-Eriksson, T., Alborn, A.-M., Nordborg, C., Peterson, D.A. & Gage, F.H. (1998) Neurogenesis in the adult human hippocampus. *Nat. Med.*, **4**, 1313–1317.

Fishell, G. & Kriegstein, A.R. (2003) Neurons from radial glia: the consequences of asymmetric inheritance. *Curr. Opin. Neurobiol.*, **13**, 34–41.

Frederickson, C.J., Kasarskis, E.J., Ringo, D. & Frederickson, R.E. (1987) A quinoline fluorescence method for visualizing and assaying the histochemically reactive zinc (bouton zinc) in the brain. *J. Neurosci. Meth.*, **20**, 91–103.

Frederickson, C.J., Suh, S.W., Silva, D., Frederickson, C.J. & Thompson, R.B. (2000) Importance of zinc in the central nervous system: the zinc-containing neuron. *J. Nutr.*, **130** (suppl.), 1471S–1483S.

Gähwiler, B.H. (1984) Development of the hippocampus in vitro: cell types, synapses and receptors. *Neuroscience*, **11**, 751–760.

Gähwiler, B.H., Capogna, M., Debanne, D., McKinney, R.A. & Thompson, S.M. (1997) Organotypic slice cultures: a technique has come of age. *Trends Neurosci.*, **20**, 471–477.

Goldman, S. (2003) Glia as neural progenitor cells. *Trends Neurosci.*, **26**, 590–596.

Gould, E., Beylin, A., Tanapat, P., Reeves, A. & Shors, T.J. (1999a) Learning enhances adult neurogenesis in the hippocampal formation. *Nat. Neurosci.*, **2**, 260–265.

Gould, E. & Gross, D.G. (2002) Neurogenesis in adult mammals: some progress and problems. *J. Neurosci.*, **22**, 619–623.

Gould, E., Reeves, A.J., Fallah, M., Tanapat, P. & Gross, C.G. (1999b) Hippocampal neurogenesis in adult Old World primates. *Proc. Natl. Acad. Sci. USA*, **96**, 5263–5267.

Gould, E. & Tanapat, P. (1997) Lesion-induced proliferation of neuronal progenitors in the dentate gyrus of the adult rat. *Neuroscience*, **80**, 427–436.

Gutierrez, R. & Heinemann, U. (1999) Synaptic reorganization in explanted cultures of rat hippocampus. *Brain Res.*, **815**, 304–316.

Hastings, N.B. & Gould, E. (1999) Rapid extension of axons into the CA3 region by adult-generated granule cells. *J. Comp. Neurol.*, **413**, 146–154.

Hayes, N.L. & Nowakowski, R.S. (2002) Dynamics of cell proliferation in the adult dentate gyrus of two inbred strains of mice. *Dev. Brain Res.*, **134**, 77–85.

Henze, D.A., Urban, N.N. & Barrionuevo, G. (2000) The multifarious hippocampal mossy fiber pathway: a review. *Neuroscience*, **98**, 407–427.

Kempermann, G. (2002) Why new neurons? Possible functions for adult hippocampal neurogenesis. *J. Neurosci.*, **22**, 635–638.

Kempermann, G., Kuhn, H.G. & Gage, F.H. (1997) More hippocampal neurons in adult mice living in an enriched environment. *Nature*, **386**, 493–495.

Kornack, D.R. & Rakic, P. (1999) Continuation of neurogenesis in the hippocampus of the adult macaque monkey. *Proc. Natl. Acad. Sci. USA*, **96**, 5768–5773.

Kronenberg, G., Reuter, K., Steiner, B., Brandt, M.D., Jessberger, S., Yamaguchi, M. & Kempermann, G. (2003) Subpopulations of proliferating cells of the adult hippocampus respond differently to physiologic neurogenic stimuli. *J. Comp. Neurol.*, **467**, 455–463.

Kuhn, H.G., Dickinson-Anson, H. & Gage, F.H. (1996) Neurogenesis in the dentate gyrus of the adult rat: age-related decrease of neuronal progenitor proliferation. *J. Neurosci.*, **16**, 2027–2033.

Kuhn, H.G., Palmer, T.D. & Fuchs, E. (2001) Adult neurogenesis: a compensatory mechanism for neuronal damage. *Eur. Arch. Psychiatry Clin. Neurosci.*, **251**, 152–158.

Landau, N.R. & Littman, D.R. (1992) Packaging system for rapid production of murine leukemia virus vectors with variable tropism. *J. Virol.*, **66**, 5110–5113.

Lee, M.K., Rebhun, L.I. & Frankfurter, A. (1990) Posttranslational modification of class III beta-tubulin. *Proc. Natl. Acad. Sci. USA*, **87**, 7195–7199.

Lendahl, U., Zimmerman, L.B. & McKay, R.D. (1990) CNS stem cells express a new class of intermediate filament protein. *Cell*, **60**, 585–595.

Liu, J., Solway, K., Messing, R.O. & Sharp, F.R. (1998) Increased neurogenesis in the dentate gyrus after transient global ischemia in gerbils. *J. Neurosci.*, **18**, 7768–7778.

Ludwin, S.K., Kosek, J.C. & Eng, L.F. (1976) The topographical distribution of S-100 and GFA proteins in the adult rat brain: an immunohistochemical study using horseradish peroxidase-labelled antibodies. *J. Comp. Neurol.*, **165**, 197–207.

Markakis, E.A. & Gage, F.H. (1999) Adult-generated neurons in the dentate gyrus send axonal projections to field CA3 and are surrounded by synaptic vesicles. *J. Comp. Neurol.*, **406**, 449–460.

Menezes, J.R. & Luskin, M.B. (1994) Expression of neuron-specific tubulin defines a novel population in the proliferative layers of the developing telencephalon. *J. Neurosci.*, **14**, 5399–5416.

Miyaguchi, K. (1997) Ultrastructure of intermediate filaments of nestin- and vimentin-immunoreactive astrocytes in organotypic slice cultures of hippocampus. *J. Struct. Biol.*, **120**, 61–68.

Mullen, R.J., Buck, C.R. & Smith, A.M. (1992) NeuN, a neuronal specific nuclear protein in vertebrates. *Development*, **116**, 201–211.

Okada, M., Sakaguchi, T. & Kawasaki, K. (1995) Correlation between anti-ubiquitin immunoreactivity and region-specific neuronal death in *N*-methyl-D-aspartate-treated rat hippocampal organotypic cultures. *Neurosci. Res.*, **22**, 359–366.

Palmer, T.D., Takahashi, J. & Gage, F.H. (1997) The adult rat hippocampus contains primordial neural stem cells. *Mol. Cell. Neurosci.*, **8**, 389–404.

Palmer, T.D., Willhoite, A.R. & Gage, F.H. (2000) Vascular niche for adult hippocampal neurogenesis. *J. Comp. Neurol.*, **425**, 479–494.

van Praag, H., Schinder, A.F., Christie, B.R., Toni, N., Palmer, T.D. & Gage, F.H. (2002) Functional neurogenesis in the adult hippocampus. *Nature*, **415**, 1030–1034.

Raineteau, O., Rietschin, L., Gradwohl, G., Guillemot, F. & Gähwiler, B.H. (2004) Neurogenesisi in hippocampal slice cultures. *Mol. Cell. Neurosci.*, **26**, 241–250.

Rakic, P. (2002) Adult neurogenesis in mammals: An identity crisis. *J. Neurosci.*, **22**, 614–618.

Robain, O., Barbin, G., Billette de Villemeur, T., Jardin, L., Jahchan, T. & Ben-Ari, Y. (1994) Development of mossy fiber synapses in hippocampal slice culture. *Dev. Brain Res.*, **80**, 244–250.

Sakaguchi, T., Okada, M. & Kawasaki, K. (1994) Sprouting of CA3 pyramidal neurons to the dentate gyrus in rat hippocampal organotypic cultures. *Neurosci. Res.*, **20**, 157–164.

Seri, B., Garcia-Verdugo, J.M., McEwen, B.S. & Alvarez-Buylla, A. (2001) Astrocytes give rise to new neurons in the adult mammalian hippocampus. *J. Neurosci.*, **21**, 7153–7160.

Shors, T.J., Miesegaes, G., Beylin, A., Zhao, M., Rydel, T. & Gould, E. (2001) Neurogenesis in the adult is involved in the formation of trace memories. *Nature*, **410**, 372–376.

Song, H.-J., Stevens, C.F. & Gage, F.H. (2002) Neural stem cells from adult hippocampus develop essential properties of functional CNS neurons. *Nat. Neurosci.*, **5**, 438–445.

Stoppini, L., Buchs, P.A. & Muller, D. (1991) A simple method for organotypic cultures of nervous tissue. *J. Neurosci. Meth.*, **37**, 173–182.

Tamamaki, N., Nakamura, K., Furuta, T., Asamoto, K. & Kaneko, T. (2000) Neurons in Golgi-stain-like images revealed by GFP-adenovirus infection in vivo. *Neurosci. Res.*, **38**, 231–236.

Varea, E., Ponsoda, X., Molowny, A., Danscher, G. & Lopez-Garcia, C. (2001) Imaging synaptic zinc release in living nervous tissue. *J. Neurosci. Meth.*, **110**, 57–63.

Vogt, K., Mellor, J., Tong, G. & Nicoll, R. (2000) The actions of synaptically released zinc at hippocampal mossy fiber synapses. *Neuron*, **26**, 187–196.

Zimmer, J. & Gähwiler, B.H. (1984) Cellular and connective organization of slice cultures of the rat hippocampus and fascia dentata. *J. Comp. Neurol.*, **228**, 432–446.

Zufferey, R., Nagy, D., Mandel, R.J., Naldini, L. & Trono, D. (1997) Multiply attenuated lentiviral vector achieves efficient gene delivery in vivo. *Nat. Biotechnol.*, **15**, 871–875.

Cross-Talk between Activated Human NK Cells and CD4$^+$ T Cells via OX40-OX40 Ligand Interactions[1]

Alessandra Zingoni,*† Thierry Sornasse,[2‡] Benjamin G. Cocks,‡ Yuetsu Tanaka,§ Angela Santoni,† and Lewis L. Lanier[3]*

It is important to understand which molecules are relevant for linking innate and adaptive immune cells. In this study, we show that OX40 ligand is selectively induced on IL-2, IL-12, or IL-15-activated human NK cells following stimulation through NKG2D, the low affinity receptor for IgG (CD16) or killer cell Ig-like receptor 2DS2. CD16-activated NK cells costimulate TCR-induced proliferation, and IFN-γ produced by autologous CD4$^+$ T cells and this process is dependent upon expression of OX40 ligand and B7 by the activated NK cells. These findings suggest a novel and unexpected link between the natural and specific immune responses, providing direct evidence for cross-talk between human CD4$^+$ T cells and NK receptor-activated NK cells. ***The Journal of Immunology,*** **2004, 173: 3716–3724.**

For an effective T cell response at least two signals are needed: the first is delivered by TCR interaction with MHC and peptide, and the second involves ligation of costimulatory receptors. Costimulation can involve augmenting cell proliferation, cell survival, and/or the production of cytokines. Many receptors have now been described to be costimulatory, including receptors of the Ig superfamily, such as CD28 and ICOS, and receptors of the TNF superfamily. Interactions between TNF ligands and TNFR family members, including for example OX40 ligand (OX40L) and OX40, have been implicated in T cell costimulation (1). Expression of OX40L is inducible and has been reported on several hemopoietic cell types, including dendritic cells (2), B cells (3), T cells, and microglial cells, as well as on vascular endothelial cells (4). OX40L expression is induced on APCs several days after activation by CD40L-CD40 interactions or by inflammatory stimuli (1, 2). Recently, high levels of OX40L have been shown to be expressed on a new type of CD3$^-$CD4$^+$ accessory cell, located in B cell follicles, capable of promoting survival of Th2 cells through OX40-OX40L interactions (5). OX40 is expressed predominantly by activated CD4$^+$ T cells (6). OX40$^+$ cells are found in the T cell zones of lymphoid organs following priming with Ag (3), and also have been detected in situ in several inflammatory states, including experimental autoimmune encephalomyelitis, rheumatoid arthritis, chronic synovitis, graft-vs-host disease, and on tumor-infiltrating lymphocytes (6–9). Ligation of OX40 on CD4$^+$ T cells by agonist reagents can increase clonal expansion and cytokine production (10), enhance memory T cell development (11), and augment anti-tumor immunity (12). OX40 has also been shown to play an important role in the stimulation of anti-viral CD4$^+$ T cell responses in vivo (13).

NK cells are lymphocytes that provide innate immunity against tumors and virus-infected cells. A balance of signals received from multiple activating and inhibitory receptors regulates their effector functions (14). These receptors allow NK cells to rapidly survey their environment for danger. When an imbalance in signaling favors activation, secretion of cytokines and/or release of cytotoxic granules occurs (14). In humans, NKG2D is one of the activating receptors that is expressed on NK cells, γδ T cells, and CD8αβ T cells (15). NKG2D recognizes as ligands UL16-binding protein 1 (ULBP1), ULBP2, ULBP3, ULBP4, and the MHC class I chain-related molecules, MICA and MICB (15, 16). These NKG2D ligands are generally absent or expressed at low levels on most healthy cells, but can be induced by viral (17) and bacterial infections (18, 19). In addition, they are frequently up-regulated in many epithelial tumors (20) and in "stressed" cells (21).

Several studies have focused on the ability of NK cells to regulate adaptive immune responses through the production of Th1-type cytokines early during infection (22) or through the activation of dendritic cells (23). In addition, by establishing cocultures of NK- and Ag-activated T cells, it has been shown that human NK cells can be induced to secrete IFN-γ in response to IL-2 produced by activated T cells (24). In contrast, much less has been reported about the physical interactions that may take place between NK cells and adaptive immune cells, in particular CD4$^+$ T cells.

In this study, we show that OX40L can be induced on human NK cells by stimulation through their activating NK receptors. In addition, we present direct evidence for cross-talk between CD4$^+$ T cells and NK cells in which OX40-OX40L and CD28-B7 interactions contribute to T cell proliferation and IFN-γ production in response to TCR-induced activation.

Materials and Methods

Reagents, cytokines, Abs, and flow cytometry

Human rIL-12 and IL-15 were purchased from BioSource International (Camarillo, CA). The National Cancer Institute Biological Resources

*Department of Microbiology and Immunology and the Cancer Research Institute, University of California, San Francisco, CA 94143; †Department of Experimental Medicine and Pathology, University of Rome "La Sapienza", Rome, Italy; ‡Incyte Corporation, Palo Alto, CA 94304; and §Department of Immunology, Graduate School and Faculty of Medicine, University of the Ryukyus, Okinawa, Japan

Received for publication May 18, 2004. Accepted for publication June 18, 2004.

The costs of publication of this article were defrayed in part by the payment of page charges. This article must therefore be hereby marked *advertisement* in accordance with 18 U.S.C. Section 1734 solely to indicate this fact.

[1] L.L.L. is an American Cancer Society Research Professor, and A.Z. was a recipient of an American-Italian Cancer Foundation Fellowship and of a research contract with the University of Rome "La Sapienza". These studies were supported by National Institutes of Health Grant CA89294 and a grant from Associazione Italiana per la Ricerca sul Cancro to A.S.

[2] Current address: Protein Design Labs, Inc., Pre-Clinical and Clinical Development Sciences, 34801 Campus Drive, Fremont, CA 94555.

[3] Address correspondence and reprint requests to Dr. Lewis L. Lanier, Department of Microbiology and Immunology and the Cancer Research Institute, University of California, 513 Parnassus Avenue, San Francisco, CA 94143. E-mail address: lanier@itsa.ucsf.edu

[4] Abbreviations used in this paper: OX40L, OX40 ligand; cIg, control Ig; SEB, staphylococcal enterotoxin B; ULBP, UL16-binding protein; KIR, killer cell Ig-like receptor.

0022-1767/04/$02.00

Branch Preclinical Repository (Frederick, MD) generously provided human rIL-2. Staphylococcal enterotoxin B (SEB) and PHA were purchased from Sigma-Aldrich (St. Louis, MO). The following mouse anti-human mAbs were used: anti-killer cell Ig-like receptor (KIR)2DS2 (DX27), neutralizing anti-CD80 (L307), and anti-CD86 (IT2.2) (BD Pharmingen, San Diego, CA), FITC-conjugated anti-CD80 (BU63; Caltag Laboratories, Burlingame, CA), FITC-conjugated anti-CD86 (MEM-233; Caltag Laboratories), anti-CD8α (Leu2a; BD Pharmingen), anti-CD4 (Leu3a; BD Pharmingen), anti-HLA-DR (BD Pharmingen), anti-NKG2D (clone 149810; R&D Systems, Minneapolis, MN), anti-CD56 (DX32), neutralizing anti-OX40L (5A8) (2, 4), anti-CD16 (B73.1) (kindly provided by Dr. G. Trinchieri, Schering-Plough, Dardilly, France), and anti-CD3 (OKT3; American Tissue Culture Collection, Manassas, VA). PE-conjugated goat anti-mouse IgG was purchased from Jackson ImmunoResearch Laboratories (West Grove, PA), FITC-conjugated anti-mouse IgG was purchased from Zymed Laboratories (South San Francisco, CA), and goat anti-mouse IgG F(ab')$_2$ was from Cappel Laboratories (ICN Biomedicals, Opera, Milan, Italy). Cells were analyzed by using a FACSCalibur (BD Biosciences, San Jose, CA) or a small desktop Guava Personal Cytometer with Guava ViaCount and Guava Express software (Burlingame, CA). Viable lymphocyte populations were gated based on forward and side scatters and by propidium iodide staining.

Cell lines, plasmids, and transfectants

The NKL cell line, generously provided by Dr. Mike Robertson (25), was cultured in RPMI 1640 medium supplemented with 10% FCS, 2 mM L-glutamine, 100 U/ml penicillin, 100 μg/ml streptomycin, and 200 U/ml human rIL-2. Cells were cultured at a density of 5×10^5/ml in a 37°C incubator with 5% CO_2. For all experiments, cells were grown at a density of 1×10^6/ml in medium containing IL-2. Generation of NKL stably expressing KIR2DS2 was described previously (26). Because mouse Ba/F3 pro-B cells are IL-3 dependent for their proliferation, the Ba/F3 cells used in these experiments were transfected with an expression plasmid containing the mouse cDNA IL-3 to provide for autocrine growth (kindly provided by Dr. S. Tangye, Centenary Institute, Sydney, Australia). MICA transfectants were established by retroviral transduction using the pMX-pie vector (27, 28) containing a MICA*0019 cDNA.

Preparation of NK cells and T cells

Small resting $CD4^+$ T lymphocytes were purified as follows: PBMC were isolated by lymphoprep density gradient centrifugation, monocytes and B cells were removed by adherence to nylon wool, then cells were labeled with anti-CD8, anti-CD56, anti-HLA-DR, and anti-CD19 mAbs, and these cells were mixed with magnetic beads coated with goat anti-mouse IgG (Dynal Biotech, Oslo, Norway). Thereafter, $CD8^+$, $CD19^+$, $HLA\text{-}DR^+$, and $CD56^+$ cells were removed by magnetic cell sorting. The remaining cells were >98% $CD4^+CD3^+$, as assessed by immunofluorescence and flow cytometric analysis. Polyclonal NK cell cultures were obtained by coculturing nylon nonadherent PBMC with irradiated (3000 rad) RPMI 8866 B cells for 9–10 days at 37°C in a humidified 5% CO_2 atmosphere, as previously described (29). NK cell cultures were >90% $CD16^+CD56^+CD3^-$, as assessed by immunofluorescence and flow cytometric analysis. Contaminating T cells were depleted by magnetic cell sorting, yielding a final NK population >98% $CD16^+CD56^+CD3^-$.

Stimulation of the cells, RNA preparation, microarrays, and data analysis

Twenty-four-well culture plates were coated with goat anti-mouse IgG (5 μg/ml, in carbonate buffer, pH 9.6) at 37°C for 4 h. Wells were washed three times with PBS and primary Abs were added to each well at 10 μg/ml, or amounts indicated in the figures, and incubated overnight at 4°C in PBS. When in combination with anti-NKG2D mAb, anti-KIR2DS2 mAb was used at 0.5 μg/ml. NKL cells were plated at 2×10^6/ml in each well in 500 μl of medium. Poly(A)$^+$ RNA was isolated using an mRNA isolation kit (Qiagen, Valencia, CA) according to the manufacturer's protocol. Gene expression modulation between unstimulated and stimulated NKL cells was evaluated by using Incyte standard procedures (Palo Alto, CA), as described elsewhere (30). Briefly, poly(A)$^+$ RNA were labeled with Cy3 or Cy5 fluorescent labeling dyes using reverse transcription, followed by hybridization onto a Human Drug Target 1 microarray (Incyte) (31, 32). This microarray contained a total of 9129 elements representing a total of 8481 unique gene clusters whose identity was confirmed by stringent PCR verification during manufacturing. The Cy3/Cy5 ratio for each element was considered valid if the signal to background ratios for both dyes exceeded 2.5, and if the signal of either dye exceeded 250 fluorescence units. A total of 6125 elements returned valid Cy3/Cy5 ratios for all 20 hybridizations (10 treatments hybridized in duplicates). Elements were further selected based on a minimum Cy3/Cy5 ratio of 2-fold in either direction in at least one experimental condition, yielding 406 elements of interest. These elements of interest were then clustered using an agglomerative clustering algorithm (Ward's method, JMP; SAS Institute, Cary, NC). All data are expressed in $\log_2$, where negative values denote gene up-regulation (Cy3 < Cy5) and reciprocally, positive values represent gene down-regulation (Cy3 > Cy5).

Cytokine and proliferation assays

Homogeneous populations of cultured human primary NK cells were activated for 72 h with IL-2 (100 U/ml) and stimulated with anti-CD16 plate-bound mAb for 18 h. In some experiments, NK cells were preactivated with IL-15 (10 ng/ml) or IL-12 (10 U/ml). Dead cells were removed by Ficoll-gradient centrifugation. NK cells were fixed with 1% paraformaldehyde (in PBS, pH 7.4) for 7 min at room temperature. Different numbers of NK cells were plated with 1×10^5 highly purified autologous $CD4^+$ T cells, and cultured for 5 days in the presence of soluble anti-CD3 mAb (5 μg/ml) or SEB (0.5–25 ng/ml) or PHA (50 ng/ml). Blocking Ab against OX40L and/or CD80 and CD86 was added on day 0 at 5 μg/ml. Wells were pulsed with 0.5 μCi of [^{3}H]thymidine for the final 18 h of culture, and incorporated radioactivity was measured in a scintillation counter. Data are represented as the mean of cpm ± SD (triplicates). In some experiments, supernatants were collected at day 3 or 5, and the amount of IL-4 and IFN-γ was quantified by specific ELISA kits (BioSource International).

Results

Microarray analysis shows up-regulation of OX40L following triggering of NK-activating receptors on a human NK cell line

Microarray analysis was used to characterize genes up-regulated by the stimulation of NKG2D alone or in combination with the DAP12-associated KIR2DS2-activating receptor. As a model, we used a human NK cell line, NKL, which constitutively expresses the DAP10-associated NKG2D receptor (33), and was transfected with KIR2DS2 (26). Because NKG2D alone is an insufficient stimulus for the transcription-dependent production of IFN-γ (26, 34), this cell system is particularly useful because it provided the opportunity to evaluate the efficacy of NKG2D costimulation using as a read out the amplification of KIR2DS2-induced IFN-γ (Ref. 26 and data not shown). Poly(A)$^+$ mRNA from resting and stimulated NKL cells was extracted, and cDNA was prepared for the comprehensive analysis of gene transcription by using microarray technology. A Human Drug Target 1 Incyte microarray containing a total of 9128 elements was used. Analysis of data was performed using a hierarchical clustering algorithm to group genes with similar expression patterns across all the samples. We focused our attention on a group of seven genes that were amplified significantly following the simultaneous cross-linking of KIR2DS2 and NKG2D receptors (Table I). These genes included three chemokines (i.e., lymphotactin, MIP-1β, and CCL18), granzymes B and H, the platelet-activating receptor homologue (a seven transmembrane receptor of unknown function), and the TNF member OX40L (CD134L). Among this group of genes, OX40L mRNA was the only one that was up-regulated by NKG2D cross-linking alone (Table I). Previously, OX40L expression has been implicated predominantly in the function of APCs, such as activated monocytes, dendritic cells, and B cells. Thus, this unexpected finding prompted us to investigate the role of OX40L in human NK cell function.

Results from the microarray experiment were confirmed by showing that cross-linking KIR2DS2, NKG2D, and KIR2DS2 plus NKG2D indeed enhanced transcription of OX40L in NKL cells, as determined by quantitative RT-PCR analysis (data not shown). More importantly, KIR2DS2- and NKG2D-induced activation resulted in an increased expression of OX40L on the cell surface of NKL cells, as determined by using a specific anti-OX40L mAb

Table 1. *Microarray analysis of NKL cells stimulated through NKG2D and/or KIR2DS2*[a]

Gene Name	Accession Number	cIg	KIR2DS2	NKG2D	KIR2DS2 + NKG2D
Lymphotactin	AL031736	0.31	−0.85	0.48	−2.39
MIP-1β	AV758471	0.06	−1.03	−0.07	−2.14
Granzyme H	NM_004131	0.43	−0.58	0.96	−1.87
Granzyme B	M57888	0.12	−0.48	0.81	−1.74
PAR	NM_013308	0.32	−0.72	0.07	−1.63
OX40L	**BE349175**	**0.13**	**−0.68**	**−0.20**	**−1.26**
CCL18	NM_00298	0.48	−0.58	0.14	−1.42

[a] Differential expression ratios of control Ig (cIg)-treated NKL cells (Cy3) compared to anti-KIR2DS2 and/or anti-NKG2D-treated NKL cells (Cy5) expressed in $\log_2$. Negative values represent up-regulation of transcription compared with cIg-stimulated cells.

(Fig. 1*A*). Stimulation with high doses of anti-KIR mAb or anti-NKG2D mAb alone substantially up-regulated OX40L on the surface of NKL cells. In addition, anti-NKG2D mAb augmented up-regulation of OX40L on NKL cells stimulated with a suboptimal dose of anti-KIR mAb (Fig. 1*A*).

OX40 is expressed predominantly on activated $CD4^+$ T cells and prior studies have shown that interactions between OX40 on activated $CD4^+$ T cells and OX40L on APCs can augment T cell proliferation and cytokine production. Therefore, studies were performed to determine whether OX40L-bearing NK cells could costimulate $CD4^+$ T cell proliferation. NKL cells, which constitutively express OX40L (Fig. 1*A*), were cocultured with freshly isolated human $CD4^+$ T cells and were stimulated with anti-CD3 mAb or PHA. As shown in Fig. 1*B*, NKL indeed augmented $CD4^+$ T cell proliferation, and this activity was blocked, in part, in the presence of a neutralizing anti-OX40L mAb. These studies indicated that OX40L on NKL is functional and contributes to the proliferation of $CD4^+$ T cells. However, these studies were complicated by the necessity to use allogeneic $CD4^+$ T cells and also because NKL is a long-term NK cell line established from a patient with NK cell leukemia (25). Therefore, it was important to validate these findings using autologous NK cells and T cells from normal healthy individuals.

Both cytokines and NK receptor-mediated stimulation are required to induce OX40L on human peripheral blood NK cells

Freshly isolated, highly purified human peripheral blood NK cells do not express OX40L on the cell surface (data not shown), although a prior study had reported the presence of OX40L transcripts (35). Because the NKL cell line requires IL-2 for growth, we investigated whether OX40L could be induced on peripheral blood NK cells from healthy adults simply by culture in the presence of IL-2 or other cytokines known to stimulate NK cells, e.g., IL-12 and IL-15. As shown in Fig. 2*A*, culture of normal human peripheral blood NK cells in IL-2, IL-12, or IL-15 failed to induce OX40L. Therefore, based on the observation that OX40L was up-regulated in NKL cells stimulated through its activating receptors, we stimulated human polyclonal NK cells through CD16, an IgG FcR that signals via the ITAM-bearing FcεRIγ and CD3ζ adapter proteins. Whereas treatment with cytokines alone failed to induce OX40L, the majority (typically 60% or more) of normal NK cells stimulated by plate-bound anti-CD16 mAb together with IL-2, IL-12, and IL-15 expressed OX40L at high levels on the cell surface (Fig. 2*A*). Stimulation with anti-CD16 mAb in the absence of IL-2 (or IL-12 or IL-15) induced OX40L only on a small proportion of NK cells. A dose-dependent induction of OX40L was observed when NK cells were activated with anti-CD16 mAb in the presence of IL-2 (Fig. 2*B*). In contrast to OX40L, culture of peripheral blood NK cells in IL-2 only did induce expression of CD86 (Fig. 2*C*) and this was not enhanced by stimulation with anti-CD16 mAb (Fig. 2*D*). CD80, another ligand of the CD28 costimulatory receptor on T cells, was not induced by IL-2 (Fig. 2*C*), and there was only a very slight indication of CD80 induction when both IL-2 and anti-CD16 stimulation were combined (Fig. 2*D*).

Because studies using the NKL cell line indicated that stimulation through the NKG2D receptor up-regulated OX40L, we also investigated this using peripheral blood NK cells from healthy adults. Polyclonal populations of NK cells from healthy individuals were expanded in culture, preactivated with IL-2 and stimulated with a plate-bound mAb against NKG2D. Fig. 3*A* shows that NKG2D cross-linking induced OX40L on ~20% of the NK cells.

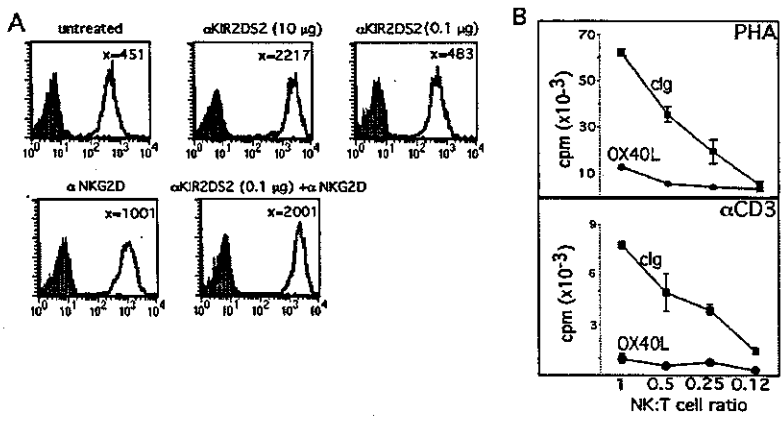

FIGURE 1. Up-regulation of OX40L on NKL by NK receptors and costimulation of $CD4^+$ T cell proliferation. *A*, NKL cells were stimulated with plate-bound mAb anti-NKG2D (10 μg/ml), anti-KIR2DS2 (10 μg/ml or 0.1 μg/ml), or both for 18 h. Cells were harvested and stained with PE-conjugated anti-OX40L mAb (open histograms) or with an isotype-matched cIg (filled histograms). *B*, Different amounts of paraformaldehyde-fixed NKL cells were cultured with 1×10^5 $CD4^+$ T cells in the presence of soluble anti-CD3 (5 μg/ml) or PHA (50 ng/ml). Neutralizing anti-OX40L mAb was added at day 0 and cocultures were harvested at day 5. Cultures were pulsed with 0.5 μCi of [^{3}H]thymidine for the final 18 h, and incorporated radioactivity was measured in a scintillation counter. A representative experiment of three is shown. Data are represented as the mean of cpm ± SD.

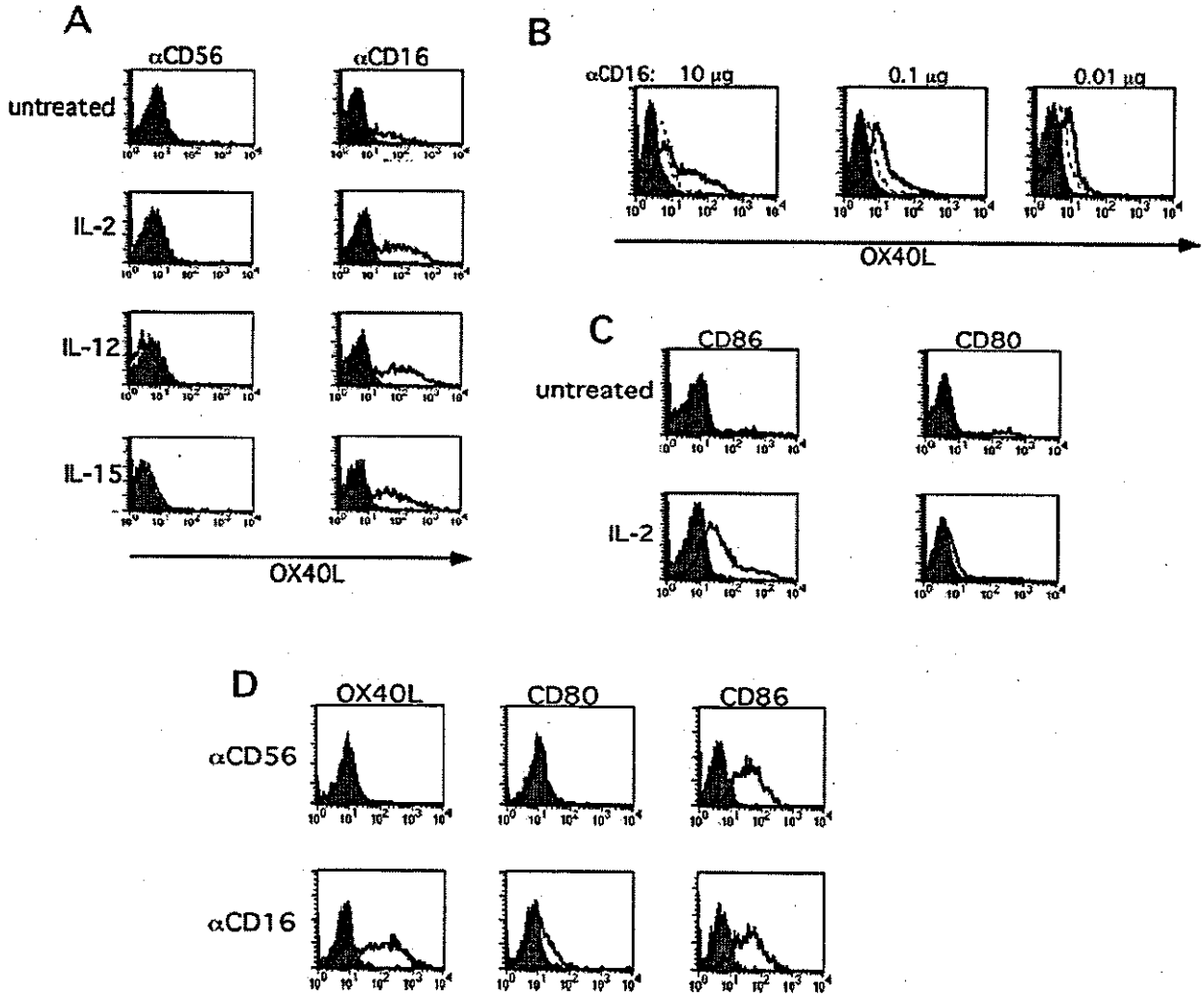

FIGURE 2. Induction of OX40L and B7 family members on human NK cells. *A*, Polyclonal human NK cells were preactivated with IL-2 (200 U/ml), IL-15 (10 ng/ml), or IL-12 (10 U/ml) for 48 h, and stimulated with plate-bound anti-CD16 mAb (saturating concentration). Plate-bound anti-CD56 mAb was used as a negative control. After 18 h of culture, cells were harvested and stained with PE-conjugated anti-OX40L mAb (thick line, open histograms) or with a cIg (filled histograms). *B*, IL-2-activated polyclonal NK cells were stimulated with different amounts (10 μg/ml, 0.1 μg/ml, and 0.01 μg/ml) of plate-bound anti-CD16 mAb (thick line). Plate-bound anti-CD56 mAb (dotted line) was used as a negative control for stimulation. Cells were harvested after 18 h and stained with FITC-conjugated anti-OX40L mAb (open histograms) or a cIg (filled histograms). A representative experiment of five is shown. *C*, Peripheral blood NK cells were cultured in the presence of IL-2 (200 U/ml) for 72 h and stained with FITC–conjugated anti-CD80 (thick lines, open histograms), FITC–conjugated anti-CD86 (thick lines, open histograms), or a cIg (filled histograms). *D*, IL-2-activated polyclonal NK cells were stimulated for 18 h with anti-CD16 or anti-CD56 (negative control) plate-bound mAbs. Cells were stained with PE-conjugated anti-OX40L mAb, FITC–conjugated anti-CD80 (thick lines, open histograms), FITC–conjugated anti-CD86 (thick lines, open histograms), or a cIg (filled histograms). In this experiment, CD86 was induced on these NK cells by coculture in IL-2, but was not further increased by stimulation with the anti-CD56 mAb used as a control.

As observed with anti-CD16 stimulation, induction of OX40L required both pretreatment with IL-2 and NKG2D activation because neither condition alone induced OX40L (data not shown). The ability of NKG2D stimulation to induce OX40L on NK cells was further validated by activation using stimulator cells bearing MICA, a physiological ligand of the NKG2D receptor. IL-2-preactivated peripheral blood NK cells were cocultured for 18 h with different ratios of the mouse pro-B cell line Ba/F3 or Ba/F3 cells stably expressing human MICA. As with anti-NKG2D mAb stimulation, OX40L was induced on ~20% of the IL-2-activated NK cells cocultured with $MICA^+$Ba/F3 cells, but not the untransfected Ba/F3 cells (Fig. 3*B*). Analysis of the kinetics of OX40L expression on human NK cells following stimulation with MICA-bearing cells showed that OX40L expression was transient; it was expressed rapidly after 5 h, peaked at 18 h, and then declined between 32 to 48 h poststimulation (Fig. 3*C*). These IL-2-activated NK cells were able to efficiently kill the $MICA^+$Ba/F3 cells, but not the untransfected Ba/F3 cells, demonstrating that the NKG2D receptor on the NK cells was specifically activated (data not shown).

Therefore, both by stimulation with anti-NKG2D mAb and by interaction with $MICA^+$Ba/F3 cells, we observed induction of OX40L on a subset comprising ~20% of IL-2-activated peripheral blood NK cells (Fig. 3). An examination of the phenotype of the NK cells stimulated by either anti-NKG2D or $MICA^+$Ba/F3 cells revealed that OX40L was induced on both the $CD56^{bright}CD16^{-/low}$ and on the $CD56^{int}CD16^{high}$ peripheral blood NK cell subsets, although within these subsets a relatively higher fraction of the $CD56^{bright}CD16^{-/low}$ NK cells expressed OX40L (our unpublished observation). Therefore, the subset of peripheral blood NK cells presenting OX40L after NKG2D stimulation was not

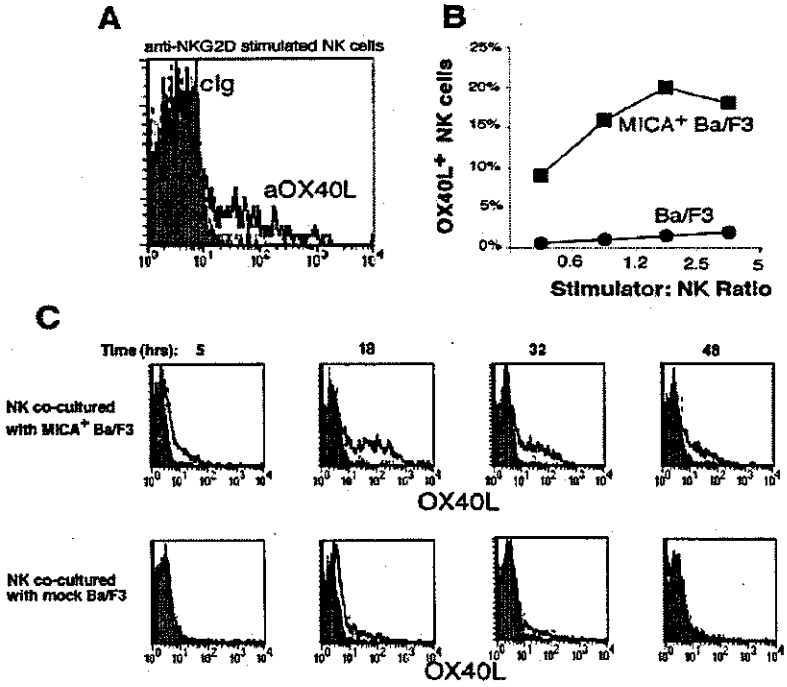

FIGURE 3. NKG2D stimulation induces OX40L on human polyclonal NK cells. *A*, Polyclonal human NK were activated with IL-2 for 72 h and stimulated with plate-bound anti-NKG2D mAb (thick line). Anti-CD56 mAb was used as a negative control of stimulation (dotted line). After 18 h of culture, cells were harvested and stained with FITC-conjugated anti-OX40L mAb (thick line, open histogram) or with cIg (filled histogram). A representative experiment of six is shown. *B*, IL-2-activated polyclonal NK cells were cultured with different numbers of mock Ba/F3 (●) or human MICA$^+$Ba/F3 (■) transfectants. After 18 h of coculture, NK cells were stained with anti-OX40L or control mAbs and the percentage of OX40L$^+$ NK cells is shown. A representative experiment of three is shown. *C*, Kinetics of OX40L induction on NK cells by coculture with NKG2D ligand-bearing cells. IL-2-activated polyclonal NK cells were cultured at a 1:2.5 stimulator:NK cell ratio with mock Ba/F3 (*lower panels*) or MICA$^+$Ba/F3 (*upper panels*) transfectants. Cells were harvested after 5, 18, 32, and 48 h of coculture, and stained anti-OX40L mAb (thick line, open histograms) and cIg (filled histograms). A representative experiment of three is shown.

restricted to either of these functionally distinct subsets defined by levels of CD56 and CD16 expression. In experiments combining both anti-NKG2D and anti-CD16 mAb stimulation (using optimal and saturating concentrations of both mAbs), the proportion of peripheral blood NK cells that expressed OX40L was equivalent to using optimal stimulation with anti-CD16 alone (data not shown).

NK cell costimulation of TCR-dependent CD4$^+$ T cell proliferation via OX40L-OX40 interactions

Our preliminary studies demonstrated that the OX40L$^+$ NKL leukemic cells were able to augment the proliferation of allogeneic human resting peripheral blood CD4$^+$ T cells stimulated with anti-CD3 mAb or PHA. The proliferation was partially, but substantially, inhibited by using a neutralizing anti-OX40L mAb (Fig. 1*B*). To address the potential interactions between NK cells CD4$^+$ T cells in a more physiological context, we performed additional experiments using autologous NK cells and CD4$^+$ T cells. We assayed proliferation induced not only by anti-CD3 mAb, but also by using autologous activated human NK cells (that express HLA-DR) to present SEB to autologous resting CD4$^+$ T cells. Because we had determined that anti-CD16 was more efficient than anti-NKG2D for inducing OX40L on peripheral blood NK cells, this system was chosen to evaluate the role of OX40L in the interactions between NK cells and autologous CD4$^+$ T cells. Highly purified, IL-2-preactivated peripheral blood NK cells were stimulated with anti-CD16 mAb, the NK cells were paraformaldehyde-fixed to prevent their proliferation or secretion of cytokines, and these cells were cocultured at varying ratios with highly purified resting autologous CD4$^+$ T cells in the presence of soluble anti-CD3 mAb. As shown in Fig. 4*A*, CD16-activated autologous NK cells efficiently costimulated anti-CD3-induced proliferation of CD4$^+$ T cells. This TCR-induced T cell proliferation was in part dependent upon OX40–OX40L interactions, because the proliferation was inhibited on average 60% (based on experiments using NK and T cells from seven different blood donors), in cultures containing the anti-OX40L specific neutralizing mAb 5A8. IL-2-activated NK cells that did not express OX40L were also able to costimulate the anti-CD3-induced proliferation of autologous CD4$^+$ T cells; however, this was always of a lower magnitude (approximately one third) than when the NK cells expressed OX40L as a consequence of prior stimulation via CD16 (Fig. 4*B*). An analysis of cytokines produced in these cultures revealed that the NK cell-costimulated T cells produced IFN-γ, but not IL-4 (Fig. 4*C*). Similar to the effects observed in the proliferation assays, anti-OX40L partially, but substantially, inhibited IFN-γ secretion induced by NK cell costimulation. In these experiments, fixed activated NK cells were used for costimulation to avoid the proliferation of the NK cells in response to IL-2, confirming that CD4$^+$ T cells were the responding population in the cultures, and to exclude that NK cell-derived cytokines were required for costimulation. We also established autologous NK:T cell cocultures with irradiated NK cells, and similar to fixed activated NK cells, irradiated activated NK also efficiently costimulated T cell proliferation in a OX40–OX40L dependent manner (data not shown).

Next, we investigated the role of OX40-OX40L interactions in autologous NK:T cell cocultures in response to a physiological TCR ligand, rather than anti-CD3 mAb. Bacterial superantigens bind with high affinity to MHC class II Ags on APCs and with TCR β-chains on the responding T cells. This results in the T cell activation responsible for toxic shock syndrome and food poisoning. Activated NK cells express MHC class II molecules (36, 37) and present SEB to T lymphocytes (37). Thus, anti-CD16-activated MHC class II-positive NK cells and autologous freshly isolated resting CD4$^+$ T cells were cultured in the presence of different concentrations of SEB. As shown in Fig. 5*A*, activated NK cells efficiently present SEB to autologous CD4$^+$ T cells, stimulating T cell proliferation. Furthermore, OX40-OX40L interactions were required for optimal T cell proliferation, as shown in Fig. 5*B* by the ability of anti-OX40L mAb to substantially inhibit SEB-induced T cell proliferation. Collectively, these data indicate that CD16-activated NK cells can efficiently costimulate anti-CD3 or SEB-induced proliferation of autologous CD4$^+$ T cells, and that OX40L-OX40 interactions are critically involved.

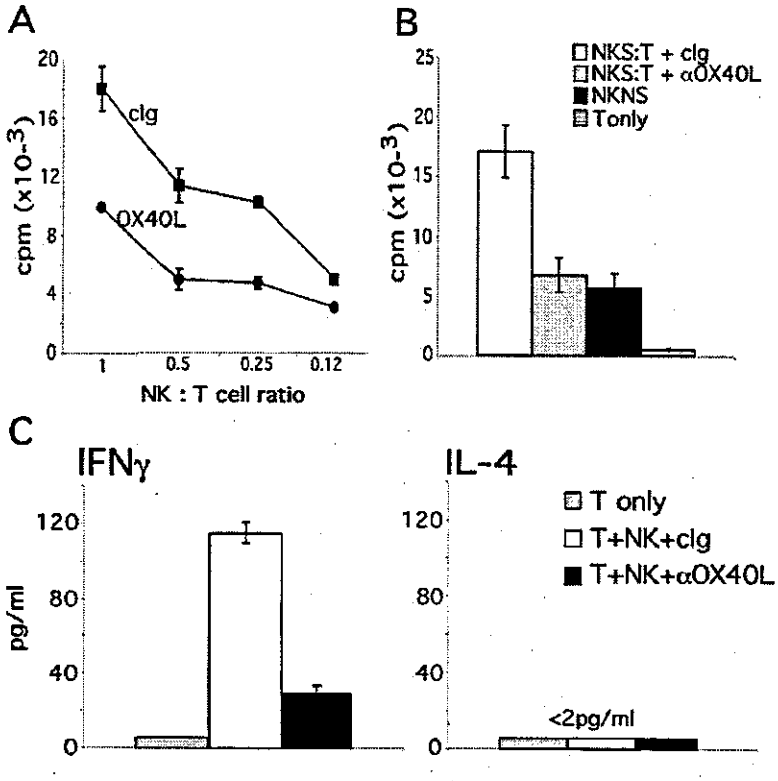

FIGURE 4. Anti-CD3 induced $CD4^+$ T cell proliferation and IFN-γ production costimulated by OX40L on autologous CD16-activated NK cells. *A*, IL-2-activated polyclonal NK cells were stimulated with plate-bound anti-CD16 mAb and fixed with 1% paraformaldehyde. Different numbers of anti-CD16-activated NK cells were plated with 1×10^5 autologous resting $CD4^+$ T cells in the presence of soluble anti-CD3 and cultured as described in Fig. 1*B*. Neutralizing anti-OX40L mAb or a cIg was added at day 0. A representative experiment of four is shown. Data are represented as the mean of cpm ± SD (triplicates). *B*, Cocultures of autologous activated NK cells and resting $CD4^+$ T cells at a ratio of 1:1 were established as described in Fig. 4*A*, using anti-CD16-stimulated NK cells (NKS) or cIg (anti-CD56 mAb)-treated NK cells (NKNS). Neutralizing anti-OX40L mAb or a cIg was added to the coculture of NKS and autologous $CD4^+$ T cells stimulated with anti-CD3, as indicated. Data are represented as the mean of cpm ± SE of seven independent experiments. *C*, Activated NK cell-resting $CD4^+$ T cell cocultures stimulated with anti-CD3 mAb were established as described in Fig. 4*A*. Neutralizing anti-OX40L mAb or a cIg was added to the cocultures, as indicated. Supernatants were collected after 72 h and tested for the presence of IFN-γ or IL-4. Data are represented as the mean ± SD (triplicates). A representative experiment of three is shown.

OX40L and B7 contribute to NK cell costimulation of $CD4^+$ T cell

We considered that the inability of anti-OX40L mAb to completely block $CD4^+$ T cell proliferation induced by activated NK cells may be due to the presence of CD86 (and perhaps CD80) on the activated NK cells (Fig. 2, *C* and *D*). Therefore, additional experiments were performed in which CD16-stimulated NK cells were cocultured with autologous $CD4^+$ T cells and anti-CD3 using a mixture of neutralizing mAbs against CD80 and CD86 (38) alone or in combination with anti-OX40L (Fig. 6). Interestingly, while mAbs against CD80 plus CD86 or OX40L individually partially inhibited NK cell-induced T cell proliferation, we observed that the combination of neutralizing mAbs against CD80, CD86, and OX40L completely blocked TCR-dependent $CD4^+$ T cell proliferation (results from two different blood donors are shown and are representative of five experiments). Collectively, these data show that CD16-stimulated NK cells efficiently costimulate TCR-dependent $CD4^+$ T cell proliferation through the expression of OX40L and B7-family members on the CD16-activated NK cells.

Discussion

Although it has been appreciated that NK cell production of IFN-γ and possibly other cytokines and chemokines can affect innate and adaptive immune responses, the potential role for direct cell-cell interactions between NK cells and T lymphocytes, in particular $CD4^+$ T cells, has not been explored. Roncarolo and colleagues (39) previously reported that human NK cell clones are able to stimulate autologous $CD4^+$ T cells, but the molecules involved in this process were not defined. Our unexpected finding that OX40L was up-regulated when NK cell receptors were stimulated on a transformed NK cell line prompted us to re-evaluate how activated NK cells are able to augment the TCR-dependent proliferation of resting autologous peripheral blood $CD4^+$ T cells. In this study, we provide evidence that activated human NK cells are able to help TCR-stimulated autologous $CD4^+$ T cells by a process that involves both OX40L and B7 costimulation.

Resting peripheral blood NK cells express neither OX40L nor B7, and different stimuli are required to induce these costimulatory molecules. Culture in IL-2 alone was sufficient to induce CD86, but not OX40L. By contrast, stimulation with IL-2 and activation through an NK receptor was required to induce OX40L. In addition to IL-2, IL-12 and IL-15 were also able to prime NK cells such that they up-regulated OX40L when subsequently stimulated via CD16. Because IL-12 and IL-15 are innate cytokines that may be more available at a site of inflammation or an ongoing immune response, these may represent the more physiologically relevant cytokines in vivo.

With respect to the NK receptors that induced OX40L, our first clues were derived from studies of the transformed NKL cell line. Although this cell constitutively expressed OX40L, it can be up-regulated by engaging either the DAP12-associated KIR2DS2 receptor that activates the Syk and ZAP70 tyrosine kinase pathways (40), or by stimulating the DAP10-associated NKG2D receptor that uses a PI3K-dependent activation pathway (33). We do not have Abs that can discriminate between the activating and inhibitory KIR; therefore, in studies of peripheral blood NK cells, we stimulated the NK cells with anti-CD16, which couples to the ITAM-bearing FcεRIγ and CD3ζ adapter proteins and activates Syk and ZAP70. When IL-2-preactivated peripheral blood NK cells were stimulated with either anti-CD16 or anti-NKG2D (or exposed to cells expressing the NKG2D ligand, MICA), OX40L was rapidly induced. Interestingly, only a subset comprising ~20% of the peripheral blood NK cells expressed OX40L after stimulating NKG2D, despite the fact that essentially all of the NK cells expressed NKG2D. Further studies are needed to determine why expression of OX40L was confined to a subset of the NKG2D-activated NK cells. By contrast, a much larger frequency of NK cells (typically 60% or more) expressed OX40L after CD16

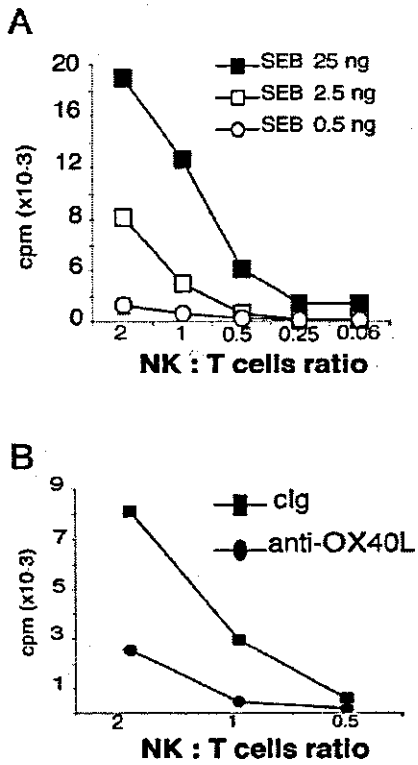

FIGURE 5. OX40L expressed on autologous NK receptor-activated NK cells is involved in SEB-induced proliferation of $CD4^+$ T cells. *A*, Anti-CD16-activated NK cells were prepared as described in Fig. 4*A*. Autologous resting $CD4^+$ T cells and activated NK cells were cocultured for 5 days in the presence of different concentrations of SEB, as indicated. Data are represented as the mean of cpm ± SD (triplicates). A representative experiment of two is shown. *B*, Autologous resting $CD4^+$ T cells and anti-CD16-activated NK cells at the indicated ratios were cocultured in the presence of 2.5 ng/ml SEB for 5 days. Neutralizing anti-OX40L mAb or cIg was added at day 0. Data are represented as the mean of cpm ± SD (triplicates). A representative experiment of three is shown.

activation. Many of the NK receptors, e.g., NKp30, NKp44, NKp46, CD16, and the activating KIR (41), use ITAM-based adapter proteins to activate the Syk/ZAP70 tyrosine kinases. Therefore, we suspect that OX40L may be induced when any of these diverse receptors are engaged because they use a common downstream signaling pathway. Together with the ability of IL-2, IL-12, or IL-15 to render the NK cells permissive for NK receptor induction of OX40L, our findings indicate that OX40L may be available in many different physiological situations for potential interactions with T cells bearing OX40.

Where might activated NK cells and $CD4^+$ T cells interact? This interaction might happen in peripheral tissues such as the liver in which both NK cells and T cells are resident (42) and accumulate following virus infection (43). Furthermore, a recent report has revealed that NK cells are relatively abundant in the human secondary lymphoid organs (44), and importantly, immunohistochemistry studies have detected NK cells in the parafollicular T cell areas of human lymph nodes (24), providing another possible location in which NK:T cell interactions might occur during an immune response. During a viral or bacterial infection, NK cells in the lymph nodes may be exposed to an environment containing IL-2, IL-12, or IL-15, and potential NKG2D ligands or immune complexes (that engage CD16), thereby providing the stimuli needed for induction of OX40L and allowing them to interact with activated $CD4^+$ T cell-expressing OX40.

It should be appreciated that activated human NK cells express high levels of MHC class II (36, 37), which provides them the potential to present Ag to human $CD4^+$ T cells. Indeed, in these studies, we have shown that activated NK cells have the capability to directly stimulate $CD4^+$ T cell proliferation by presenting SEB to $CD4^+$ T cells. Therefore, activated human NK cells possess not only the required costimulatory molecules (e.g., OX40L and B7) for potential interaction with activated $CD4^+$ cells, but they also, in theory, have the capacity of present Ags via MHC class II. Collectively, our in vitro experiments provide compelling evidence that human NK cells and autologous $CD4^+$ cells can interact and that OX40L is an important participant in this process. It is difficult to provide formal proof of this interaction in vivo in humans. Unfortunately, because activated mouse NK cells (unlike human NK cells) do not express MHC class II, mice do not provide a relevant or appropriate model to examine MHC class II TCR-dependent $CD4^+$ cell interactions with NK cells. Although dendritic cells are considered the most potent APCs, the fact that activated NK cells express MHC class II, CD86, and OX40L strongly suggests the possibility that they may also communicate directly with $CD4^+$ cells. Otherwise, for what purpose would NK receptor-activated human NK cells express MHC class II, CD86, and OX40L?

Our findings demonstrate that human NK cell costimulation of TCR-induced $CD4^+$ T proliferation depends in a large part on OX40–OX40L interactions. Studies conducted using OX40-deficient mice have shown that OX40-deficient $CD4^+$ T cells initially become activated to secrete IL-2 (albeit at slightly lower levels than wild-type mice), but they are unable to sustain proliferation (45). Other studies performed on $OX40^{-/-}$ mice reported that the impaired in vitro proliferative response to anti-CD3 stimulation

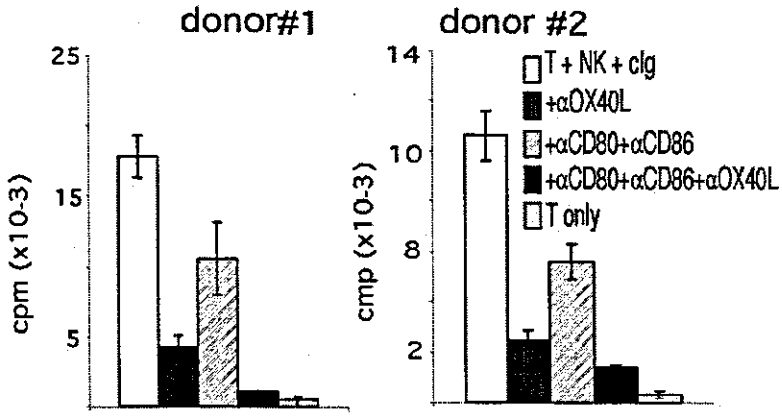

FIGURE 6. NK cell costimulation of TCR-dependent $CD4^+$ T cell proliferation involves B7 family members. Cocultures of anti-CD16-stimulated autologous NK and $CD4^+$ T cells at a ratio of 1:1 were established and stimulated with anti-CD3 as described in Fig. 4*A*. Neutralizing mAbs against CD80, CD86, and/or OX40L or cIg, as indicated, were added on day 0 at 5 μg/mL Data are represented as the mean ± SD (triplicates). Two representative experiments of five are shown.

could not be corrected by the addition of exogenous rIL-2 (46). Most significantly, it has been shown that OX40 is a major regulator of anti-apoptotic proteins, such as Bcl-xL and Bcl-2 (45), and strongly promotes the survival of Ag-activated primary $CD4^+$ T cells (11). Similarly, the contribution of OX40-OX40L interactions to T cell proliferation that we have observed may favor T cell survival by the induction of Bcl-xL and Bcl-2, although this awaits further evaluation.

Previous studies reported that OX40L expressed on mouse B cells induce a Th2-type response, leading to the expansion of IL-4-producing mouse T effector cells and inhibiting IFN-γ expression (47, 48). In humans, a role for OX40L in the development of Th2 effector cells has also been reported (49). However, other studies do not support a differential role for OX40L in inducing Th1 vs Th2 differentiation (11, 13, 50, 51). suggesting that it only enhances the pre-existing response. In our studies using activated human NK cells to costimulate autologous $CD4^+$ T cells, we observed the production of IFN-γ, but not IL-4 secretion, by the TCR-activated T cells. These findings suggest that activated, mature human NK cells may preferentially promote T cell IFN-γ production.

We believe that the induction of OX40L on NK cells by NKG2D ligand-expressing cells might have important implications in the context of tumor surveillance and infectious diseases. It has been shown that the NKG2D ligand MICA is up-regulated on several human tumor cells and, interestingly, soluble MICA has been found in the serum of patients affected by different progressive tumors (52). In addition, several studies have reported that MICA is induced on cells infected with *Mycobacteria tuberculosis* (18), *Escherichia coli* (19), or cytomegalovirus (17). Thus, initial interactions between NK cells and NKG2D ligand-bearing cells or soluble NKG2D ligands may trigger killing and cytokine production and in the presence of IL-2, IL-15, or IL-12 may induce expression of OX40L on the NK cells. Subsequent interactions between $OX40L^+$ NK cells and $OX40^+$ T cells may amplify and sustain an adaptive ongoing immune response. At least under the experimental conditions used, we observed the induction of OX40L only on a subset of activated human peripheral blood NK cells. Further studies are necessary to resolve why some NK cells, but not others, expressed OX40L upon NKG2D stimulation, because all NK cells express NKG2D on the cell surface.

The OX40-OX40L interaction has been shown to induce bidirectional signals. For example, OX40L stimulation by OX40 transduces a signal in dendritic cells, which results in enhanced TNF-α and IL-1β production (2). Similarly, triggering of OX40L expressed on activated B cells results in B cell proliferation and Ig secretion (53). Finally, engagement of OX40L on vascular endothelial cells leads to the induction of c-*fos* and c-*jun* mRNA expression and the production of the chemokine RANTES (54, 55). Thus, while our present studies have focused on the potential role of OX40L on NK cell interactions with $CD4^+$ T cells, it will also be of interest to examine whether engagement of OX40L on NK cells might regulate their effector functions.

Acknowledgments

We thank Dr. Nigel Killeen and Dr. Cristina Cerboni for helpful discussion.

References

1. Croft, M. 2003. Co-stimulatory members of the TNFR family: keys to effective T-cell immunity? *Nat. Rev. Immunol. 3:609.*
2. Ohshima, Y., Y. Tanaka, H. Tozawa, Y. Takahashi, C. Maliszewski, and G. Delespesse. 1997. Expression and function of OX40 ligand on human dendritic cells. *J. Immunol. 159:3838.*
3. Stuber, E., and W. Strober. 1996. The T cell-B cell interaction via OX40-OX40L is necessary for the T cell dependent humoral immune response. *J. Exp. Med. 183:979.*
4. Imura, A., T. Hori, T. Imada, T. Ishikawa, Y. Tanaka, M. Maeda, S. Imamura, and T. Uchiyama. 1996. The human OX40/gp34 system directly mediates adhesion of activated T cells to vascular endothelial cells. *J. Exp. Med. 183:2185.*
5. Kim, M. Y., F. Gaspal, H. Wiggett, F. McConnell, A. Gulbranson-Judge, R. C., L. Walker, M. Goodall, and P. Lane. 2003. $CD4^+CD3^-$ accessory cells costimulate primed CD4 T cells through OX40 and CD30 at sites where T cells collaborate with B cells. *Immunity 18:643.*
6. Weinberg, A. D. 2002. OX40: targeted immunotherapy — implications for tempering autoimmunity and enhancing vaccines. *Trends Immunol. 23:102.*
7. Brugnoni, D., A. Bettinardi, F. Malacarne, P. Airo, and R. Cattaneo. 1998. CD134/OX40 expression by synovial fluid $CD4^+$ T lymphocytes in chronic synovitis. *Br. J. Rheumatol. 37:584.*
8. Tittle, T. V., A. D. Weinberg, C. N. Steinkeler, and R. T. Maziarz. 1997. Expression of the T-cell activation antigen, OX-40, identifies alloreactive T cells in acute graft-versus-host disease. *Blood 89:4652.*
9. Vetto, J. T., S. Lum, A. Morris, M. Sicotte, J. Davis, M. Lemon, and A. Weinberg. 1997. Presence of the T-cell activation marker OX-40 on tumor infiltrating lymphocytes and draining lymph node cells from patients with melanoma and head and neck cancers. *Am. J. Surg. 174:258.*
10. Gramaglia, I., A. D. Weinberg, M. Lemon, and M. Croft. 1998. Ox-40 ligand: a potent costimulatory molecule for sustaining primary CD4 T cell response. *J. Immunol. 161:6510.*
11. Gramaglia, I., A. Jember, S. D. Pipping, A. D. Weinberg, N. Killeen, and M. Croft. 2000. The OX40 costimulatory receptor determines the development of CD4 memory by regulating primary clonal expansion. *J. Immunol. 165:3043.*
12. Weinberg, A. D., M. M. Rivera, R. Prell, A. Morris, T. Ramstad, J. T. Veto, W. J. Urba, G. Alvord, C. Bunce, and J. Shields. 2000. Engagement of the OX40 receptor in vivo enhances antitumour immunity. *J. Immunol. 164:2160.*
13. Kopf, M., C. Ruedi, N. Schimitz, A. Gallimore, K. Lefrang, B. Ecabert, B. Odermatt, and M. F. Bachmann. 1999. Ox40–deficient mice are defective in Th cell proliferation but are competent in generating B cell and CTL responses after virus infection. *Immunity 11:699.*
14. Lanier, L. L. 2001. On guard: activating NK receptors. *Nat. Rev. Immunol. 2:3.*
15. Bauer, S., V. Groh, J. Wu, A. Steinle, J. H. Phillips, L. L. Lanier, and T. Spies. 1999. Activation of NK cells and T cells by NKG2D, a receptor for stress-inducible MICA. *Science 285:727.*
16. Cosman, D., J. Mullberg, C. L. Sutherland, W. Chin, R. Armitage, W. Fanslow, M. Kubin, and N. J. Chalupny. 2001. ULBPs, novel MHC class I-related molecules, bind to CMV glycoprotein UL16 and stimulate NK cytotoxicity through the NKG2D receptor. *Immunity 14:123.*
17. Groh, V., R. Rhinehart, J. Randolf-Habecker, M. S. Topp, S. R. Riddell, and T. Spies. 2001. Costimulation of CD8 $\alpha\beta$ T cells by NKG2D via engagement by MIC induced on virus-infected cells. *Nat. Immunol. 2:255.*
18. Das, H., V. Groh, C. Kuij, M. Sugita, C. T. Morita, T. Spies, and J. F. Bukowski. 2001. MICA engagement by human Vg2Vd2 T cells enhances their antigen-dependent effector function. *Immunity 15:83.*
19. Tieng, V., D. Bougu'enec, L. Du Merle, P. Bertheau, P. Desreumaux, A. Janin, D. Charron, and A. Toubert. 2002. Binding of *Escherichia coli* adhesin AfaE to CD55 triggers cell-surface expression of the MHC class I-related molecule MICA. *Proc. Natl. Acad. Sci. USA 99:2977.*
20. Groh, V., R. Rhinehart, H. Secrist, S. Bauer, A. Greght, and T. Spies. 1999. Broad tumour-associated expression and recognition by tumour derived $\gamma\delta$ T cells of MICA and MICB. *Proc. Natl. Acad. Sci. USA 96:6879.*
21. Groh, V., S. Bahram, S. Bauer, A. Herman, M. Beauchamp, and T. Spies. 1996. Cell stress–regulated human major histocompatibility complex class I gene expressed in gastrointestinal epithelium. *Proc. Natl. Acad. Sci. USA 93:12445.*
22. Biron, C. A., K. B. Nguyen, G. C. Pien, L. P. Cousens, and T. P. Salazar-Mather. 1999. Natural killer cells in antiviral defence: function and regulation by innate cytokines. *Annu. Rev. Immunol. 17:189.*
23. Moretta, A. 2002. Natural Killer cells and dendritic cells: rendezvous in abused tissues. *Nat. Rev. Immunol. 2:957.*
24. Fehniger, T. A., M. A. Cooper, G. J. Nuovo, M. Cella, F. Facchetti, M. Colonna, and M. Caligiuri. 2003. $CD56^{bright}$ natural killer cells are present in human lymph nodes and are activated by T cell-derived IL-2: a potential new link between adaptive and innate immunity. *Blood 101:3052.*
25. Robertson, M. J., K. J. Cochran, C. Cameron, J. M. Le, R. Tantravahi, and J. Ritz. 1996. Characterization of a cell line, NKL, derived from an aggressive human natural killer cell leukemia. *Exp. Hematol. 24:406.*
26. Wu, J., H. Cherwinski, T. Spies, J. H. Phillips, and L. L. Lanier. 2000. DAP10 and DAP12 form distinct, but functionally cooperative, receptor complexes in natural killer cells. *J. Exp. Med. 192:1059.*
27. Kinsella, T. M., and G. P. Nolan. 1996. Episomal vectors rapidly and stably produce high-titer recombinant retrovirus. *Hum. Gene Ther. 7:1405.*
28. Onishi, M., S. Kinoshita, Y. Morikawa, A. Shibuya, J. Phillips, L. L. Lanier, D. M. Gorman, G. P. Nolan, A. Miyajima, and T. Kitamura. 1996. Applications of retrovirus-mediated expression cloning. *Exp. Hematol. 24:324.*
29. Zingoni, A., G. Palmieri, S. Morrone, M. Carretero, M. Lopez-Botet, M. Piccoli, L. Frati, and A. Santoni. 2000. CD69-triggered ERK activation and functions are negatively regulated by CD94/NKG2-A inhibitory receptor. *Eur. J. Immunol. 30:644.*
30. De Risi, J. L., V. R. Iyer, and P. O. Brown. 1997. Exploring the metabolic and genetic control of gene expression on a genomic scale. *Science 278:680.*
31. Bandman, O., R. T. Coleman, J. F. Loring, J. J. Seilhamer, and B. G. Cocks. 2002. Complexity of inflammatory responses in endothelial cells and vascular

smooth muscle cells determined by microarray analysis. *Ann. NY Acad. Sci. 975:77.*
32. Yue, H., P. S. Eastman, B. B. Wang, J. Minor, M. H. Doctolero, R. L. Nuttall, R. Stack, J. W. Becker, J. R. Montgomery, M. Vainer, and R. Johnston. 2001. An evaluation of the performance of cDNA microarrays for detecting changes in global mRNA expression. *Nucleic Acids Res. 29:41.*
33. Wu, J., Y. Song, A. B. Bakker, S. Bauer, T. Spies, L. L. Lanier, and J. H. Phillips. 1999. An activating immunoreceptor complex formed by NKG2D and DAP10. *Science 285:730.*
34. Billadeau, D. D., J. L. Upshaw, R. A. Schoon, C. J. Dick, and P. J. Leibson. 2003. NKG2D-DAP10 triggers human NK cell-mediated killing via a Syk-independent regulatory pathway. *Nat. Immunol. 4:557.*
35. Kashii, Y., R. Giorda, R. B. Herberman, T. L. Whiteside, and N. L. Vujanovic. 1999. Constitutive expression and role of TNF family ligands in apoptotic killing of tumor cells by human NK cells. *J. Immunol. 163:5358.*
36. Phillips, J. H., A. M. Le, and L. L. Lanier. 1984. Natural killer cells activated in a human mixed lymphocyte response culture identified by expression of Leu-11 and class II histocompatibility antigens. *J. Exp. Med. 159:993.*
37. D'Orazio, J. A., and J. Stein-Streilein. 1996. Human natural killer cells present staphylococcal enterotoxin B (SEB) to T lymphocytes. *Clin. Exp. Immunol. 104:366.*
38. Lanier, L. L., S. O'Fallon, C. Somoza, J. H. Phillips, P. S. Linsley, K. Okumura, D. Ito, and M. Azuma. 1995. CD80 (B7) and CD86 (B70) provide similar costimulatory signals for T cell proliferation, cytokine production, and generation of CTL. *J. Immunol. 154:97.*
39. Roncarolo, M. G., M. Bigler, J. B. Haanen, H. Yssel, R. Bacchetta, J. E. de Vries, and H. Spits. 1991. Natural killer cell clones can efficiently process and present protein antigens. *J. Immunol. 147:781.*
40. Lanier, L. L., B. C. Corliss, J. Wu, C. Leong, and J. H. Phillips. 1998. Immunoreceptor DAP12 bearing a tyrosine-based activation motif is involved in activating NK cells. *Nature 391:703.*
41. Moretta, A., C. Bottino, M. Vitale, D. Pende, C. Cantoni, M. C. Mingari, R. Biassoni, and L. Moretta. 2001. Activating receptors and coreceptors involved in human natural killer cell-mediated cytolysis. *Annu. Rev. Immunol. 19:197.*
42. Crispe, I. 2003. Hepatic T cells and liver tolerance. *Nat. Rev. Immunol. 3:51.*
43. Salazar-Mather, T. P., T. A. Hamilton, and C. A. Biron. 2000. A chemokine-to-cytokine-to-chemokine cascade critical in antiviral defense. *J. Clin. Invest. 105:985.*
44. Ferlazzo, G., D. Thomas, S. L. Lin, K. Goodman, B. Morandi, W. A. Muller, A. Moretta, and C. Munz. 2004. The abundant NK cells in human secondary lymphoid tissues requires activation to express killer cell Ig-like receptors and become cytolytic. *J. Immunol. 172:1455.*
45. Rogers, P. R., J. Song, I. Gramaglia, N. Killeen, and M. Croft. 2001. OX40 promotes Bcl-xL and Bcl-2 expression and is essential for long term survival of CD4 T cells. *Immunity 15:445.*
46. Pipping, S. D., C. Pena-Rossi, J. Long, W. R. Godfrey, D. J. Fowell, S. L. Reiner, M. L. Birkeland, R. M. Locksley, A. N. Barclay, and N. Killeen. 1999. Robust B cell immunity but impaired T cell proliferation in the absence of CD134 (OX40). *J. Immunol. 163:6520.*
47. Linton, P.-J., B. Bautista, E. Biederman, E. S. Bradley, J. Harbertson, R. M. Kondrack, R. C. Patrick, and L. Bradley. 2003. Costimulation via OX40L expressed by B cells is sufficient to determine the extent of primary CD4 cell expansion and Th2 cytokine secretion in vivo. *J. Exp. Med. 197:875.*
48. Flynn, S., K.-M. Toellner, C. Raykundalia, M. Goodall, and P. Lane. 1998. CD4T cell cytokine differentiation: the B cell activation molecule, OX40L, instructs CD4T cells to express interleukin 4 and upregulates expression of the chemokine receptor, Blr-1. *J. Exp. Med. 188:297.*
49. Ohshima, Y., L.-P. Yang, T. Uchiyama, Y. Tanaka, P. Baum, M. Sergerie, P. Hermann, and G. Delespesse. 1998. Ox40 costimulation enhances interleukin-4 (IL-4) expression at priming and promotes the differentiation of naïve human $CD4^+$ T cells into high Il-4-producing effectors. *Blood 92:3338.*
50. De Smedt, T., J. Smith, P. Baum, W. Fanslow, E. Butz, and C. Maliszewski. 2002. Ox40 costimulation enhances the development of T cell responses induced by dendritic cells in vivo. *J. Immunol. 168:661.*
51. Chen, A. I., J. McAdam, J. E. Buhlmann, S. Scott, M. L. Lupher, E. A. Greenfield, P. R. Baum, W. C. Fanslow, D. M. Calderhead, G. J. Freeman, and A. H. Sharpe. 1999. OX40-ligand has a critical costimulatory role in dendritic cell:T cell interactions. *Immunity 11:689.*
52. Groh, V., J. Wu, C. See, and T. Spies. 2002. Tumour-derived soluble MIC ligands impair expression of NKG2D and T-cell activation. *Nature 419:734.*
53. Morimoto, S., Y. Kanno, Y. Tanaka, Y. Tokano, S. Hashimotò, S. Jacquot, C. Morimoto, S. F. Schlossman, H. Yagita, K. Okumura, and T. Kobata. 2000. CD134L engagement enhances human B cell Ig production: CD154/CD40, CD70/CD27, and CD134/CD134L interactions coordinately regulate T cell-dependent B cell responses. *J. Immunol. 164:4097.*
54. Matsumura, Y., T. Hori, S. Kawamata, A. Imura, and T. Uchiyama. 1999. Intracellular signaling of gp34, the OX40L: induction of c-*jun* and c-*fos* mRNA expression through gp34 upon binding of its receptor, OX40. *J. Immunol. 163:3007.*
55. Kotani, A., T. Hori, Y. Matsumura, and T. Uchiyama. 2002. Signaling of gp34 (OX40 ligand) induces vascular endothelial cells to produce a CC chemokine RANTES/CCL5. *Immunol. Lett. 84:1.*

Available online at www.sciencedirect.com
SCIENCE DIRECT®
Biochemical and Biophysical Research Communications 320 (2004) 18–26
BBRC
www.elsevier.com/locate/ybbrc

Nuclear trafficking of macromolecules by an oligopeptide derived from Vpr of human immunodeficiency virus type-1

Takashi Taguchi,[a] Mari Shimura,[a] Yoshiaki Osawa,[a] Yasunori Suzuki,[a] Izuru Mizoguchi,[a] Koitsu Niino,[b] Fumimaro Takaku,[c] and Yukihito Ishizaka[a,*]

[a] *Department of Intractable Diseases, International Medical Center of Japan, 1-21-1 Toyama, Shinjuku-ku, Tokyo 162-8655, Japan*
[b] *Niino Clinic, 1-64 Sakuragi-cho, Yonezawa, Yamagata 992-0027, Japan*
[c] *Jichi Medical School, 3311-1 Yakushiji, Minamikawachi-machi, Kawachi-gun, Tochigi 329-0498, Japan*

Received 12 March 2004
Available online 8 June 2004

Abstract

Vpr, an accessory gene product of HIV-1, is incorporated into cells when added to the culture medium. Via such function Vpr has been shown to transduce a protein into cells that is expressed as a chimeric protein with Vpr. The domain required for protein transduction, however, remained to be clarified. Here we identified a sequence encompassing 52–78 amino acids of Vpr (C45D18) that enables nuclear trafficking of proteins. When chemically synthesized C45D18 was added to the culture medium of human cord blood mononuclear (CBMN) cells, most cells became positive for the incorporated C45D18. Furthermore, recombinant proteins conjugated with the C45D18 were efficiently transduced and transported to regions corresponding to the nucleus. Incorporation of C45D18-conjugated protein was observed within a few hours after addition of the protein, independent of cellular growth. Although it is well known that Tat-derived peptide has a transducing activity, C45D18 was more active than Tat peptide for trafficking proteins into cells. Taking together with results from FACS analysis revealing that more than 90% of CBMN cells were positive for X-gal staining after treatment of C45D18-conjugated β-galactosidase, we propose that C45D18 translocates bioactive macromolecules directly into the nucleus.

Keywords: HIV-1; Vpr; Nuclear trafficking; Protein transduction domain; Resting cells

Vpr, one of six auxiliary genes of human immunodeficiency virus type 1 (HIV) [1,2] encodes a virion-associated protein [3–5], and has been proposed as a factor crucial for HIV-1 infection in resting macrophages [6]. Several lines of evidence indicate that Vpr is involved in translocation of preintegration complex from cytoplasm to nucleus [6,7]. Vpr is a small protein composed of 96 amino acids (aa), but has several functional domains of three α-helix regions (17–29, 36–47, and 53–78, respectively), a leucine-rich region from 60 to 80 aa, and C-terminal arginine-rich region [7]. It has been noted that Vpr has two separable parts responsible for nuclear translocation [8]. On the other hand, we previously reported that Vpr induces genomic instability by causing chromosome breaks and aneuploidy [9,10]. Our experiments also revealed that the C-terminal region of Vpr is important for cell-cycle arrest, and Vpr mutant lacking C-terminal 18 aa was negative for inducing cell-cycle abnormality at the G2/M phase.

As a particularly interesting property, Vpr functions like a transacting factor, and latently infected cells restart viral production, when Vpr is extracellularly added to cells [11,12]. In addition to such an activity, Vpr can enter cells when it is added to culture medium [7,13]. Consistently, a synthetic full-length peptide of Vpr or C-half of Vpr was used for efficient transduction of plasmid DNA [14]. On the other hand, Sherman et al. [15] recently reported that Vpr could transport exogenous proteins into cells. A fusion protein of Vpr with β-galactosidase (β-gal) was also shown to enter cells.

* Corresponding author. Fax: +81-3-5272-7527.
E-mail address: zakay@ri.imcj.go.jp (Y. Ishizaka).

0006-291X/$ - see front matter © 2004 Elsevier Inc. All rights reserved.
doi:10.1016/j.bbrc.2004.05.126

Such a transduction activity of Vpr is energy independent and does not require a cellular receptor [15]. As one of possibly related mechanisms of transducing activity, Vpr forms a channel in cellular membranes [16,17], and the amino-terminal region of 40 aa of Vpr with α-helix structures is responsible for the ion channel formation [17].

Proteins, such as antennapedia of *Drosophila* (ANTP) [18], VP22 of herpes simplex [19], and Tat of HIV-1 [20], are known to possess protein transduction domains (PTD). PTD enables proteins to cross biological membranes and helps them to enter the cytoplasm. It has been also reported that a variety of proteins, when expressed as chimetric proteins with the peptide, enter target cells. PTD has an arginine-rich region, and it was expected that the C-terminal region of Vpr, which contains an arginine-rich stretch, functioned as PTD. It was, however, concluded that the C-terminal half of Vpr did not show any activities as PTD [15], and the region of Vpr responsible for transducing exogenous protein remained to be clarified.

In the present study, we identified a sequence corresponding to the third α-helix domain (C45D18) as PTD. Interestingly, C45D18 entered cells even without cellular growth, and C45D18-conjugated green fluorescent protein (GFP) was quickly transferred to the nucleus. Transduction of protein conjugated with C45D18 was more efficient than that conjugated with Tat-derived peptide. Based on results that C45D18-conjugated proteins were efficiently transduced into cord blood mononuclear (CBMN) cells as well as resting adherent cells, we propose that C45D18 functions as a novel vehicle that facilitates nuclear trafficking of molecules into target cells.

Materials and methods

Cell culture and chemicals. HT1080 and HeLa cells were cultured in Dulbecco's modified Eagle's medium supplemented with 10% fetal calf serum (FCS) (Sigma, SI). Cord blood was kindly provided by volunteers who gave informed consent. CBMN cells were prepared by centrifugation, according to the manufacturer's protocol (Nycomed Pharma AS, Norway). Briefly, cord blood was diluted with the same amount of phosphate buffered saline (PBS) and applied on the Lymphoprep solution. After centrifugation for 20 min at 800*g*, cells at the interphase were collected, washed once with PBS, and resuspended in Iscove's modified Dulbecco's medium (IMDM) supplemented with 10% FCS. Jurkat cells and HL-60 cells were cultured in IMDM with 10% FCS. To prepare resting cells, HT1080 cells were cultured for 4 days in FCS-free medium. Cell growth of HL-60 cells was also arrested with 1 μg/ml aphidicolin (APC) (Sigma, SI). As a control, dimethyl sulfoxide (DMSO), used as a solvent of APC, was treated.

Peptide synthesis and detection of incorporated peptide. Various types of peptides derived from Vpr (see Fig. 1A) and Tat (GYGRKKRR QRRRGGC, amino acids described as single letters) were chemically synthesized (Wako, Tokyo). Biotin was added at the amino terminal end of each peptide. After treatment of peptides, cells were washed once with PBS and then fixed with 100% ice-cold methanol. To exclude signals associated with cellular membranes, cells were treated for 10 min with 0.2% Triton X-100 in PBS [21]. Cells were then reacted for 1 h with streptavidin (SA)-conjugated FITC (SA-FITC) and washed several times in PBS with 0.05% Tween 20. To detect the interaction of the peptide and plasmid DNA, different doses of the peptide (1–30 μg) were mixed with 0.2 μg plasmid DNA. A reporter plasmid, pCMV/luciferase, was kindly provided by Dr. Shimada (Nihon Medical School). Luciferase activity was assayed, as described [21].

Expression of recombinant green fluorescent protein and conjugation with peptides. A recombinant protein of green fluorescent protein (GFP) tagged with $(His)_6$ was expressed by a baculovirus system with pFASTBAC and purified with proband region (Invitrogen, Carlsbad, CA). Molecular weights of GFP and β-galactosidase (β-gal) (Wako, MI) were about 35 and 465 kDa, respectively. These proteins were chemically conjugated with Vpr-derived peptides (IBL, Fujioka, Japan). Briefly, about 300 μg protein was suspended in 10 mM phosphate buffer (pH 7.0) and added with 0.1 mM *N*-[e-maleimidocaproyloxiy]succinimide ester (DOJINDO Lab. Kumamoto, Japan). After 30 min at room temperature, each Vpr-derived peptide was added and further incubated for 3 h at room temperature. Conjugated molecules were then dialyzed against PBS overnight.

To test protein transduction, cells were incubated with conjugated proteins overnight and incorporated GFP was detected by an antibody. To demonstrate β-gal activity, X-gal staining was carried out according to the method described [22].

Fluorescent activated cell sorter (FACS) analysis. Incorporation of peptides was analyzed by detecting SA-FITC bound to the peptides. For cell-cycle analysis, cells were treated for 1 h with 10 μM bromodeoxyuridine (BrdU) (Sigma, St. Louis, MO). After fixation in 70% ice-cold ethanol, cells were treated with FITC-conjugated anti-BrdU antibody (Beckton–Dickinson, San Jose, CA) and then stained with 5 μM propidium iodide (Sigma). To study the effect of Vpr on cell-cycle, cells after treatment of peptides were stained with 50 μg/ml propidium iodide and subjected to FACS analysis. For FACS analysis of β-galactosidase activity, a FluoReporter lacZ Flow Cytometry Kit (Molecular Probes, Eugene, OR) was used. Briefly, 5×10^5/100 μl of CBMN cells was mixed with 1 mM fluorescein di-β-D-galactopyranoside for 1 min and was added to 1.8 ml of ice-cold PBS containing 1.5 μM propidium iodide. FACS analysis was carried out by Cellquest (Beckton–Dickinson, San Jose, CA).

Results

Identification of Vpr-derived oligopeptide with transducing activity

The carboxyl-half of Vpr has been shown to transduce plasmid DNA into cultured cells [14]. On the other hand, we previously reported that Vpr induced cell-cycle abnormality at the G2/M phase, but Vpr mutant that lacked C-terminal 18 amino acids was negative for the cell-cycle abnormality [9]. Based on these observations, we tested whether C-terminal 45 aa of Vpr without the extreme C-terminal 18 aa (C45D18, Fig. 1A) had a trafficking activity. A biotin-conjugated 27-mer peptide (52–78 aa) was synthesized, and 10 μg/ml of the peptide was added into the medium of cultured cells. On the next day, an incorporated peptide was detected with SA-FITC. As shown in Fig. 1B, C45D18 was clearly detected in the peptide-treated cells (Fig. 1B, middle

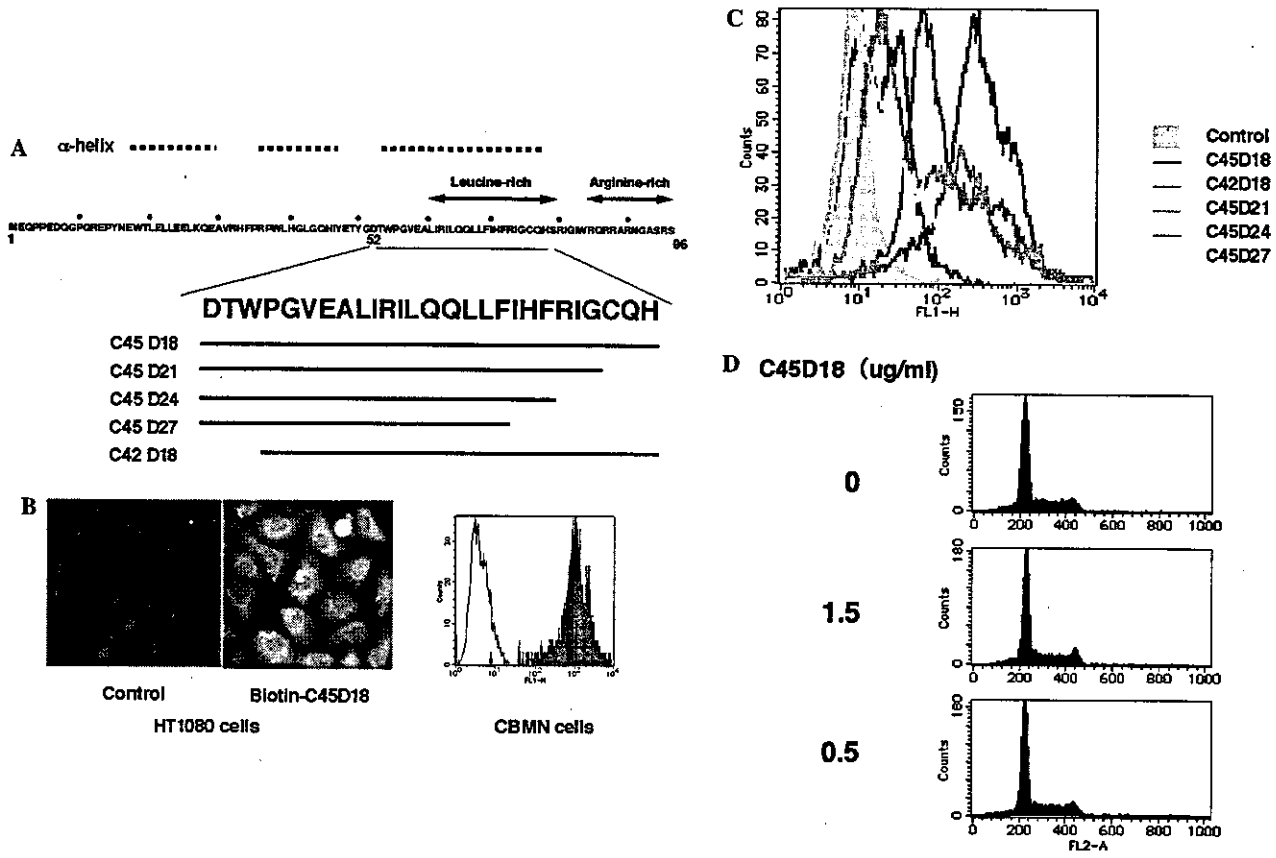

Fig. 1. Identification of Vpr-derived peptide that is incorporated into cells. (A) Amino acid sequence of Vpr used in the present study. (B) Incorporation of C45D18 into cells. Results of HT1080 cells (left panels) and CBMN cells (right panel) are shown. Note that almost all of cells are positive for the incorporated peptide (shown by yellow and red in left and right panels, respectively). (C) Transducing activity of synthetic peptides. Several biotin-conjugated peptides were synthesized and added into the culture medium of CBMN cells. On the next day, the incorporated peptides were detected with SA-FITC. Amino acid sequence of each peptide is shown in (A). (D) Effects of C45D18 on cell-cycle. Cells were treated with C45D18 for 2 days and then subjected to cell-cycle analysis. (For interpretation of the references to colour in this figure legend, the reader is referred to the web version of this paper.)

panel). We observed that C45D18 was also efficiently incorporated into CBMN cells (Fig. 1B, right panel shown by red). FACS analysis revealed that almost 100% of cells were positive for the incorporated peptide after overnight treatment.

To identify the minimal region required for such trafficking activity, several biotinylated peptides were synthesized (Fig. 1A), and we tested whether they were incorporated into CBMN cells, (Fig. 1C). Three peptides of C45D21 (52–75 aa), C45D24 (52–72 aa), and C45D27 (52–69 aa) were less efficiently incorporated to CBMN cells than C45D18 (orange, purple, and yellow peaks, respectively). When amino-terminal three amino acids were deleted from C45D18 (C42D18), its trafficking activity was greatly reduced (blue in Fig. 1C).

It has been reported that Vpr induces cell-cycle abnormality at G2/M phase, and we studied whether C45D18 has an activity on cell-cycle. As shown in Fig. 1D, FACS analysis revealed that cell-cycle was not changed after treatment for 2 days. These data imply that C45D18 is an appropriate sequence for further characterization of the potentiality for transducing activity.

Trafficking macromolecules

We next studied whether C45D18 could transduce plasmid DNA. Consistent with a previous report on the full-length peptide of Vpr [14], C45D18 interacted with plasmid DNA. Unfortunately, however, we could not obtain a favorable amount of exogenous gene expression in cells transfected with the complex (data not shown). To evaluate the activity of C45D18 to transport macromolecules into cells, we studied whether C45D18, when attached to a recombinant protein, entered cells. For this purpose, C45D18 was conjugated at various molar ratios with a purified recombinant protein of GFP and added into the culture medium. On the next day, incorporated proteins were detected. As shown in Fig. 2A, cells treated with C45D18-conjugated GFP were positive for incorporation, although the protein was not detected at all in cells treated with GFP by itself (Fig. 2A, left panel). In the present study, cells were treated with 0.2% Triton X-100 before treatment with SA-FITC. Since this procedure abolished signals associated with cellular membranes [21], our positive ob-